Genetic variation in mouse islet Ca^{2+} oscillations reveals novel regulators of islet function

Christopher H. Emfinger[1#], Lauren E. Clark[1#], Kathryn L. Schueler[1], Shane P. Simonett[1], Donnie S. Stapleton[1], Kelly A. Mitok[1], Matthew J. Merrins[2,3], Mark P. Keller[1], Alan D. Attie*[1,2]

[1]Department of Biochemistry, University of Wisconsin-Madison, Madison, WI, 53706, USA

[2] Department of Medicine, Division of Endocrinology, University of Wisconsin-Madison, Madison, WI, 53705, USA

[3]William S. Middleton Memorial Veterans Hospital, Madison, WI 53705 USA

[#]These authors contributed equally to this work

*corresponding author

For inquiries, please address correspondence to:

Alan D. Attie

543A HF DeLuca Biochemistry Laboratories, 433 Babcock Drive, Madison, WI 53706

(608) 262-1372

adattie@wisc.edu

KEYWORDS:

Islet calcium

Insulin secretion

Genetic variation

Beta cell

ABBREVIATIONS:

COBLL1	Cordon-Bleu-like Like 1
ACP1	Acid phosphatase 1
GALNS	galactosamine (N-acetyl)-6-sulfatase
PSMC3	Proteasome 26S subunit, ATPase 3
GWAS	Genome-wide association study
SNP	single-nucleotide polymorphism

ABSTRACT:

Insufficient insulin secretion to meet metabolic demand results in diabetes. The intracellular flux of Ca^{2+} into β-cells triggers insulin release. Since genetics strongly influences variation in islet secretory responses, we surveyed islet Ca^{2+} dynamics in eight genetically diverse mouse strains. We found high strain variation in response to four conditions: 1) 8 mM glucose; 2) 8 mM glucose plus amino acids; 3) 8 mM glucose, amino acids, plus 10nM GIP; and 4) 2 mM glucose. These stimuli interrogate β-cell function, α-cell to β-cell signaling, and incretin responses. We then correlated components of the Ca^{2+} waveforms to islet protein abundances in the same strains used for the Ca^{2+} measurements. To focus on proteins relevant to human islet function, we identified human orthologues of correlated mouse proteins that are proximal to glycemic-associated SNPs in human GWAS. Several orthologues have previously been shown to regulate insulin secretion (e.g. ABCC8, PCSK1, and GCK), supporting our mouse-to-human integration as a discovery platform. By integrating these data, we nominated novel regulators of islet Ca^{2+} oscillations and insulin secretion with potential relevance for human islet function. We also provide data for identifying appropriate mouse strains in which to study these regulators.

INTRODUCTION:

The majority of gene loci responsible for the genetic variation in type 2 diabetes (T2D) susceptibility affect the function of endocrine cells of pancreatic islets, primarily β-cells (1, 2). Variation in β-cell mass and β-cell function place boundaries on the capacity to respond to acute and chronic demands for insulin, such as those in overnutrition and insulin resistance (1, 2). Therefore, metabolic challenges are useful in genetic screens because the increased demand for insulin promotes the progression from normal blood glucose to diabetes in individuals with genetic variants that affect β-cells.

The collection of inbred mouse strains currently available provides us with a wide repertoire of genetic and phenotype diversity, comparable to that of the entire human population (3). Yet, the majority of mouse studies have been confined to a small handful of highly inbred strains (3, 4). It is becoming widely appreciated that gene deletions, nutritional interventions, and drug effects vary widely between mouse strains as they do in humans (3, 5). Thus, characterization of the basis for this high level of phenotype variation is a way to gain deeper insights into the pathophysiology and genetics of a wide range of physiological processes.

The pancreatic β-cell is a nutrient sensor. In response to particular nutrient stimuli (e.g. glucose, amino acids), the cells generate ATP and close ATP-dependent K^+ channels (K_{ATP}), resulting in plasma membrane depolarization. This leads to an oscillatory influx of Ca^{2+} ions, triggering insulin secretion. The process of secreting insulin and re-compartmentalizing Ca^{2+} ions consumes ATP, and the drop in the ATP/ADP ratio reopens K_{ATP} channels, repolarizing the membrane, and closing membrane Ca^{2+} channels. Consequently, oscillations in metabolism, insulin secretion, and Ca^{2+} are intrinsically linked (6-9), and the capacity to maintain functional Ca^{2+} handling has been suggested to be critical for islet compensation (10).

In this study, we utilized the extraordinary genetic and phenotypic diversity represented in the eight founder mouse strains (which we subsequently refer to as founders) used to generate the Collaborative

Cross (CC) recombinant inbred mouse panel and the Diversity Outbred (DO) stock (11, 12). These strains capture the majority of the genetic diversity of all inbred mouse strains (11, 12). While studies of these mice have provided significant insight into genetic regulators of islet function (13), determining the appropriate model system for evaluating genes of interest is often difficult as most deletion models are made in only a small number of strains such as the C57BL/6J.

We explored the diversity of nutrient-evoked islet Ca^{2+} responses across the eight founder mouse strains, revealing a remarkable diversity of Ca^{2+} oscillations. Our prior proteomics studies showed that the protein abundance from islets of the founder mouse strains is also highly diverse, as is their insulin secretory response to different stimuli (14). By correlating the strain and sex variation in protein abundance with the variation in Ca^{2+} oscillations, we identified a subset of islet proteins that are highly correlated with islet Ca^{2+} oscillations. The human orthologues of many of these proteins are encoded by genes with nearby SNPs linked to glycemic traits (e.g., fasting blood glucose, see **Table 2** for terms), as revealed in genome-wide association studies (GWAS). By integrating these data, we nominated novel regulators of islet Ca^{2+} oscillations and insulin secretion with potential relevance for human islet function. We also provide proteomic, secretory, and Ca^{2+} data for identifying appropriate mouse strains in which to study these regulators.

RESULTS

Genetics exerts a strong influence on islet Ca^{2+} responses

Glucose metabolism, β-cell Ca^{2+} flux, and insulin secretion are pulsatile, and have been found to oscillate in both humans and mice (6, 7, 15-17). Because they are interconnected, understanding the factors governing oscillation patterns can inform about the mechanisms that regulate insulin secretion (9, 18-20). To specifically explore the influence of genetic background on Ca^{2+} oscillations, we measured Ca^{2+} in islets of the eight founder strains, that together harbor as much genetic diversity as humans: A/J, C57BL/6J (B6), 129S1/SvlmJ (129), NOD/ShiLtJ (NOD), NZO/HILtJ (NZO), CAST/EiJ (CAST), PWK/PhJ (PWK), and WSB/EiJ (WSB).

All mice were maintained on a Western-style diet (WD) high in fat and sucrose for 16 weeks, prior to isolating their islets for Ca^{2+} imaging using Fura Red, a Ca^{2+}-sensitive fluorescent dye (**Figure 1A**). Using a perifusion system, we measured Ca^{2+} dynamics in response to four conditions: 1) 8 mM glucose (8G); 2) 8 mM glucose + 2 mM glutamine, 0.5 mM leucine, and 1.5 mM alanine (8G/QLA); 3) 8G/QLA + 10 nM glucose-dependent insulinotropic polypeptide (8G/QLA/GIP); and 4) 2 mM glucose (2G) (**Figure 1B**). There was a high degree of similarity between three of the five classical strains (A/J, B6, 129), which were dominated by slow oscillations (period 2-10 minutes) in 8G and 8G/QLA/GIP, and had relatively fewer islets reach plateau (continuous peak activity without oscillation) in 8G/QLA. Likewise, the wild-derived strains (CAST, WSB, and PWK) closely matched one another, while differing from the classic strains. The wild-derived mouse islets were dominated by fast oscillations (period <2 minutes) in 8G, resulting in plateaus for 8G/QLA and 8G/QLA/GIP.

Two strains stood out from the others. Islets from NOD mice showed characteristics from both the wild-derived and classic strains; slow oscillations in 8G and a sustained plateau in response to 8G/AA and 8G/QLA/GIP with fast oscillations superimposed. The NZO mice also differed from the other classic strains, likely because they were all diabetic (blood glucose >250 mg/dL). Their islets were minimally

responsive to 8G, but did respond with a strong pulse in 8G/QLA and Ca^{2+} remained elevated in 8G/QLA/GIP.

Many of the strain differences seen in the male mice were maintained in the females (**Supplemental Figure 1A**). The classic strains were once again highly similar to one another, as were the wild-derived strains. Furthermore, the NZO females, of which all but one were diabetic, mirrored the behavior of the male islets. One interesting observation that emerged from the female islets is that the NOD females displayed a greater variation in their Ca^{2+} oscillations than the NOD males (**Supplemental Figure 2**). Some of the islets maintained slow oscillations throughout the various conditions, while some demonstrated fast oscillations and plateaued similar to the wild-derived strains. Yet others appeared strikingly similar to the islets from diabetic NZO mice, despite none of the NOD mice being diabetic. Finally, the one non-diabetic female NZO displayed oscillatory behavior similar to that of the other classic strains, with clear, slow oscillations (**Supplemental Figure 1B**).

Dissecting islet Ca^{2+} dynamics

An understanding of the mechanisms regulating insulin secretion, including the roles of specific metabolic pathways, ion channels, and hormones, have been derived from the shape and frequency of islet Ca^{2+} oscillations (7, 9, 16, 18, 21-24). To elucidate strain differences in Ca^{2+} dynamics, we primarily analyzed six parameters of the Ca^{2+} waveform (**Figure 2A**): 1) peak (the top of each oscillation); 2) active duration (the length of time for each oscillation measured at half of the peak height); 3) pulse duration (the length of time for each oscillation where cytosolic Ca^{2+} is at its lowest); 4) period (the length of time between two peaks); 5) plateau-fraction (the active duration divided by the period, or the fraction of time spent in the “on” phase); and 6) silent duration (the period minus the active duration, or the length of time spent in the “off” phase). We also assessed the spectral density for every islet to extract additional information from complex oscillations where multiple components were visible (e.g. the trace in **Supplemental Figure 3A).** We analyzed each trace segment to determine the top two

frequencies contributing to the trace (1st and 2nd component frequencies, **Supplemental Figure 3B)** and their respective contributions (1st and 2nd component amplitudes). Because certain features, such as ion channels or metabolic enzymes, have known frequencies (25), extracting the top two frequencies may highlight additional information beyond that previously collected.

A representative Ca^{2+} dynamic from a female B6 islet is illustrated in **Figure 2A.** The transition from 8G to 8G/QLA resulted in an increased active duration, yielding a longer period and increased plateau fraction. For an islet that plateaued at the peak, as seen in 8G/QLA (**Figure 2B**), we computed a plateau-fraction of one, an active and pulse duration of 40 minutes (the measurement time), and a period of zero minutes. An islet that returned to baseline and ceased to oscillate, as seen in 2 mM glucose (**Figure 2B**), was determined to have a plateau-fraction, active duration, and pulse duration of zero, and a period of 40 minutes. Understanding the strain-dependence of these parameters is important for identifying underlying mechanisms, as illustrated in **Figure 2C**. While both traces have a similar active duration (blue bars), trace 1 has a longer period (red bars), resulting in an increased silent duration and a decreased plateau-fraction.

Examples of pathways altering specific components of Ca^{2+} oscillations have previously been established (**Figure 2D**) (9, 11, 18, 28, 29). For example, when K_{ATP} channels are pharmacologically closed with Tolbutamide, the silent duration is shortened, resulting in increased frequency without a change in pulse shape (upper panel). The addition of glucose leads to increased glucose metabolism and glucokinase (GK) activity (11). The resulting rise in ATP inhibits K_{ATP} channels and is used as a substrate for additional processes that affect Ca^{2+}, such as SERCA pumps (30, 31). Thus, glucose alters both the active and silent durations, resulting in a change in both frequency and shape of the Ca^{2+} oscillations (lower panel).

Average stimulated calcium levels do not correlate with insulin secretion

Average Ca^{2+} is commonly used for analyzing Ca^{2+} dynamics and is frequently assumed to be highly correlated to insulin secretion. To determine whether average Ca^{2+} is predictive of insulin secretion, we performed perifusions on islets from WSB and 129 male mice, two strains that showed similar average Ca^{2+} (**Figure 4B**), but exhibited vastly different Ca^{2+} oscillations (**Figure 1B**). WSB mice had significantly higher insulin secretion in each of the secretory conditions (**Figure 3A**), suggesting another Ca^{2+} parameter better predicts insulin secretion.

To identify parameters of the Ca^{2+} dynamics most strongly correlated to insulin secretion, we computed the correlation between the Ca^{2+} oscillation parameters and insulin secretion in similar conditions (8G, 8G/QLA, basal) for the same sexes and strains (**Figure 4A** and **Supplemental Figure 4**) (32). Consistent with our observations from the perifusion data in the WSB and 129 islets, we found that average Ca^{2+} was not strongly correlated to insulin secretion. Other metrics, such as active duration in 8G, and the silent durations in 8G/QLA, were more highly correlated to insulin secretion. Meanwhile, the 1st component frequency in 8G from the spectral density analysis was highly correlated with *decreased* insulin secretion. These metrics were also the most highly correlated with multiple clinical measures in the founder mice, particularly plasma insulin (**Figure 4B, Supplemental Figure 5**), for which silent duration in 8G/QLA/GIP had the strongest correlations.

Several parameters of the Ca^{2+} oscillatory waveform showed strong strain and sex effects. For example, basal Ca^{2+} (average Ca^{2+} in 2G, **Figure 4C**) was relatively consistent among the strains, except NZO where it was highest in islets from male mice. For the overall pulse duration (**Figure 4D**), the NZO mice were once again the highest, followed by CAST and WSB. A noticeable sex-effect was measured for the CAST mice, where male mice had a longer pulse duration than the female mice. The 1st component frequency (**Figure 4E**) is driven by the differences observed in the wild-derived strains, for which CAST has the highest frequency, followed by PWK and WSB. Finally, the trend for a sex

effect in the classic strains for silent duration (at 8G, 8G/QLA, and 8G/QLA/GIP) is absent in the NZO and wild derived mice with the former having greater silent duration in males and the latter frequently having islets plateau in response to these stimuli. These data demonstrate that genetics has a profound influence on key parameters of islet Ca^{2+} oscillations.

To explore this further, we took advantage of our previously published whole islet proteomic survey from the eight founder strains (14). To identify proteins that may underly the strain-differences in Ca^{2+} oscillations, we computed the correlation between islet protein abundance and Ca^{2+} dynamics across both sexes of the eight founder strains (**Figure 5** and **Supplemental Figure 6**). Our previous survey of islet proteomics included both sexes for all strains, except NZO males, resulting in a quantitative measure of ~4054 proteins (14). **Figure 5A** illustrates a heatmap of the correlation between islet proteins and several parameters of Ca^{2+} oscillations. Unsupervised clustering was used to show that groups of proteins showed strong positive or negative correlation to a given Ca^{2+} parameter and the correlation displays a distinct architecture. The proteins highly correlated to the 8G 1st component frequency, for example, tended to also be strongly anticorrelated to the silent duration conditions which were very similar to one another. The active and pulse durations for 8G had nearly identical correlation structure, and the conditions with the fewest highly correlated proteins were the average Ca^{2+} measures for 8G, 8G/QLA, and 8G/QLA/GIP, and the structure for these was largely inverted from the active duration conditions. Finally, despite the differences in the overall correlations between the different metrics, there were proteins that did overlap (e.g. the block of proteins with high correlation to both 8G A_D and 8G/QLA S_D) suggesting that while there were clusters of distinct proteins/pathways for any given metric some proteins may modify more than one metric.

Among the ~4045 islet proteins, 363 had high absolute correlation coefficients (r > |0.5|) to 3 or more of the parameters our data suggest most strongly correlate to insulin secretion and plasma insulin (Basal Ca^{2+}, 8G A_D, 8G P_D, 8G/QLA S_D, 8G S_D, 8G/QLA/GIP S_D). Interestingly, of the proteins

correlated to these traits, many have been previously implicated in islet biology, including PCSK1, GCK, SUR1, GLUT2, PDX1, and GLP-1 (26-34). Notably, the highly correlated proteins enriched for tissues, pathways, and transcription factors that support their role in insulin secretion (**Figure 5B**). For instance, proteins highly anti-correlated to active duration in 8G were enriched for components of oxidative metabolism and had their gene promoters enrich for binding to the islet transcription factor MAFA (33). These enrichment data provide a framework for discovering new genes of interest for their role in islet function.

Integration of mouse genetics with human GWAS to nominate novel players in islet biology

The data presented in **Figure 5A** illustrates the *correlation* between islet proteins and Ca^{2+} dynamics. Importantly, a protein strongly correlated to Ca^{2+} does not necessarily reflect a causal relationship; i.e., a change in protein abundance may or may not cause a change in the Ca^{2+} signal. To take our analysis beyond correlation, we integrated our data with human GWAS of glycemia-related traits.

First, we identified all human homologues for islet proteins strongly correlated (r > |0.5|) to one or more of the Ca^{2+} oscillatory metrics. We identified human homologues for ~2880 proteins that were correlated to Ca^{2+} in either direction for at least one of our parameters of interest. We then searched the Type 2 Diabetes Knowledge Portal (https://t2d.hugeamp.org/) for SNPs that are associated with one or more glycemia-related traits (see **Table 2**) with a P-value < 10^{-8}, and occur within ±100Kbp of the homologous gene (e.g. COBLL1, **Figure 6A**) or are on regions contacting the gene's promoter (determined using human islet promoter-capture HiC data (35)) as illustrated by ACP1 (**Figure 6B**). This yielded a list of 316 human genes strongly associated with diabetes-related SNPs, and 168 of these proteins have not been previously reported to play a key role in islet function (**Table 3**). In summary, our approach leverages the genetic diversity of the eight founder strains and human GWAS for diabetes-related traits to highlight genes that play a novel role in islet function.

Importantly, the relevance of these tools depends on the mouse model in which they are used to validate the roles of the candidate protein. To aid in the selection of mouse strain, we provide the proteomic, secretory, and Ca^{2+} data (**Figure 7,** https://doi.org/10.5061/dryad.j0zpc86jc). This will enable the user to identify proteins correlated to genes, proteins, or traits of interest, and from there, identify which strain(s) may be most appropriate for the study of their target. In the examples illustrated in **Figure 7C**, GALNS shows a high negative correlation to multiple traits including the active duration time in 8G/QLA. Strains at the extremes of this trait are also extremes with regard to protein expression for GALNS. Ones with high abundance (B6, for example) would be appropriate models for inhibition or knockout, while the CAST mice could be a comparison strain for validating the role of the protein, as they express less of it. By contrast, the silent duration traits (e.g. those expressed in 8 mM glucose) have strong influence of the NZO strain and consequently NZO may be the most appropriate strain to assess the role of some proteins (e.g. PMSC3) with regard to that metric (**Figure 7C**, lower panels).

DISCUSSION

Genetic variability drives islet function

While the development and progression of T2D is potentiated by environmental factors, an estimated 50% of disease risk is driven by genetic factors (1, 3, 36). Therefore, to study the genetic variation contributing to T2D, we utilized the eight founder mouse strains. These mice collectively contain a level of genetic diversity mirroring that seen in humans, making them an excellent model for studying genetic regulators of islet function (11, 12). We demonstrate that they also vary in their Ca^{2+} response to various insulin secretagogues, supporting the use of these mice to identify novel genes involved in regulating islet biology.

Calcium waveform analysis reveals pathways regulating islet function

Variations in Ca^{2+} dynamics are highly complex, and are the result of changes in metabolism, extra-islet signaling, and Ca^{2+} itself (6). We therefore selected stimulatory conditions to assess each of these components in islets of the eight mouse strains. 8 mM glucose was first used to survey glycolytic responses, because we have observed that several strains reliably oscillate at this glucose concentration. Furthermore, this glucose concentration remains close to the stimulatory threshold, thus reducing the possibility of oscillations plateauing if islet Ca^{2+} responses were left-shifted in any strains (21, 37, 38). We then added QLA as fuel to engage non-glycolytic mitochondrial metabolism and signaling from α-cells, providing a survey of alpha-to-beta cell communication in the islet (18, 39-41). Finally, we used GIP to interrogate the islet incretin responses and the cAMP amplification pathway (40), before returning to a low glucose concentration, enabling us to establish baseline Ca^{2+} levels.

The variation in Ca^{2+} response to these conditions can be better understood by examining the multitude of pathways regulating Ca^{2+} dynamics. As mentioned previously, altering ionic pathways involved in regulating Ca^{2+}, such as K_{ATP} channels, has a very different effect on Ca^{2+} oscillations compared to altering glycolysis. It is important to further dissect these pathways, as changing specific

components of glucose metabolism can elicit different effects. For example, increasing pyruvate kinase (PK), an enzyme involved in converting phosphoenolpyruvate (PEP) to pyruvate, and increasing GK activity both alter the active duration and the plateau-fraction. However, they do so in opposite directions (18). While both enzymes are involved in the glycolytic pathway, activating GK increases the active duration and period, while activating PK decreases those same parameters. This demonstrates the complexity of analyzing Ca^{2+} oscillations, and the importance of considering the changes in a variety of parameters, rather than focusing on just one.

The importance of analyzing a variety of Ca^{2+} parameters is further supported by the insulin secretion measurements in the male WSB and 129 mice. While average Ca^{2+} is a common metric used to predict insulin secretion, relying on only this metric would suggest that the two strains secrete insulin similarly. However, the WSB mice secreted significantly more insulin in 8G, 8G/QLA, and 8G/QLA/GIP (**Figure 3**). Based on our correlation analysis between Ca^{2+} parameters and insulin secretion across each sex and strain, active duration and pulse duration in 8G more accurately predicted insulin secretion and may be highly informative when used with other data (**Figure 4**). This is similar to results published by some other groups, suggesting that average Ca^{2+} does not correlate well with insulin secretion (42).

Strains segregate by their phylogenetic origins

Notably, several of the strains appeared to cluster together with similar responses. One such group is composed of three classical strains (A/J, B6, and 129) that had similar waveforms dominated by slow oscillations. These differed from a second group containing the wild-derived strains (CAST, WSB, and PWK) which closely matched one another and were dominated by faster oscillations.

The classic strains have been highly inbred (>150+ generations) and descend from related common ancestors, the “fancy mice.” They also have extremely low genetic diversity, with 97% of their genomes explained by fewer than 10 haplotypes (3, 43, 44). By contrast, wild-derived strains are each

independent in their parental origin, inbred for far fewer generations than the classic strains (although still at least 20), and include significant contributions from other subspecies of *Mus musculus* than the predominant subspecies (*M. m. domesticus*) in the traditional strains, particularly CAST (*M. m. castaneous)* and PWK (*M. m. musculus*) (3, 43, 44). It is thus unsurprising that the two primary Ca^{2+} response clusters were composed of the classic and wild-derived strains. Multiple loci have already been linked to islet dysfunction and differential metabolic homeostasis in the classic strains (3). Our work here highlights the promise in using wild-derived strains to unmask previously underappreciated islet phenomena, something we and others have previously shown (14, 45, 46).

While considered one of the classic strains, the NOD mice differed from the two primary clusters noted above. They displayed a combination of features from both groups and had a high degree of inter-islet variability, especially the female mice. NOD share common ancestors with the Swiss-Webster mice, which do not share parental origin with the other classic strains (43) and also display a “mixed” phenotype consisting of islet Ca^{2+} oscillations in response to glucose, with both slow and fast components (21).

Additionally, while all NOD were normoglycemic, a heterogeneous response was observed in islets from female, but not male, NOD mice. Female NOD mice are known to develop islet immune infiltration and subsequent autoimmune diabetes whereas males are largely protected from this (47). Male NOD islets were largely consistent in their Ca^{2+} waveforms. In the females, however, a high degree of heterogeneity in responses was observed across the female’s islets (**Supplemental Figure 2**). For any NOD female, some islets resembled those from NOD males in their clear oscillations, others largely lacked oscillatory behavior other than a strong pulse in response to 8G/QLA, and still others had an intermediate response. These observations may reflect varying degrees of dysfunction in the NOD female islets as the mice progress to diabetes, though we cannot say whether this results from variation in beta-cell intrinsic defects or islet immune infiltration.

The NZO mice also varied from the two clusters previously discussed. All of the male mice, and all but one of the female mice, were diabetic. The islets from the diabetic mice had reduced amplitude and oscillatory behavior, other than a single pulse in 8G/QLA. This pattern is similar to the patterns observed in many of the NOD female islets. On the other hand, islets of the one non-diabetic female NZO mouse demonstrated clear, slow oscillations (**Supplemental Figure 1B**) which was surprising given reports of low K_{ATP} abundance due to *Abcc8* mutations in the NZO (48) and the strong role of K_{ATP} channels in regulating islet Ca^{2+}(9, 30, 31, 49). While not of the same lineage as the NOD, the NZO do exhibit some autoimmune infiltration in the pancreas, and the marked difference between the non-diabetic and diabetic NZOs, along with the variation in female NOD islet responses, further suggests that intra-islet variability for the NOD mice may be the result of disease progression.

Understanding the genetic variation driving islet responses in the founders may be informative beyond these specific strains. Screens in the DO mice and similar outbred populations can track SNPs associated with trait variation to their parental inbred strain of origin. Our previous genetic screen for drivers of islet function observed that many of the quantitative trait loci (QTL) appearing for *ex vivo* islet traits had effects driven by the SNPs from the wild-derived strains as opposed to the traditional inbred groups (13). The QTL mediated by *Zfp148*, which drives Ca^{2+} and insulin secretion phenotypes in beta cells (38), also had strong strain effects from wild-derived strains (13).

Previous studies of islet Ca^{2+} have largely been confined to a handful of strains, and many studies by individual labs tend to use the strains with which they initiated their projects. While this does include a few outbred stocks (e.g. NMRI (50-52), CD-1 (7, 53, 54)), direct comparisons of these to the traditional inbred lines are rare (50), and studies of specific genes often use traditional inbred lines as wild-derived lines do not respond as well to the conventional assistive reproductive technologies required for genome editing and transgenesis (55, 56).

One study, comparing the outbred (NMRI) stock to the C57BL6/J and C57BL/6N strains (50), found that the NMRI displayed significantly lower frequencies than the C57 lines, particularly in physiological glucose ranges and had similar active periods. While highly informative, there were important differences between these studies and our studies here. Of note, the studies were done in acute slice culture, in only one sex, and the frequencies detected did not resemble the (at least for the C57 lines) the slow oscillations observed in isolated islets from these inbred strains (e.g. **Figure 1**, (18, 38)).

Integrating protein correlations to calcium and human GWAS nominates novel drivers of islet function

One limitation of our current study is that the association between islet proteins and Ca^{2+} waveforms is correlative and therefore cannot distinguish proteins that are causal for the differences in islet Ca^{2+} between strains from proteins changing as a result of these differences. One way to further dissociate the two, and to establish the relevance of likely candidates to human islet biology, is to identify whether genes encoding human orthologues of these proteins are associated with glycemic traits in humans. SNPs for glycemic traits (**Table 2**), particularly those involving insulin, suggest that alterations in these proteins may impart disease risk, which is less likely for proteins that do not play critical regulatory roles. Thus, the filter for glycemic trait association, while not definitive, suggests a likely causal role for these proteins in mediating differences in islet Ca^{2+} and therefore differences in secretion between strains. Integrating human GWAS data with the proteins most correlated to Ca^{2+} waveform parameters nominated over 647 protein candidates, of which approximately a third have been previously shown to have roles in some aspect of islet biology. These include well established drivers of insulin secretion responses, such as SUR1, GLUT2, and GNAS. Other previously unknown candidates show promise for validation, as they are already targets of small molecule compounds (e.g. ACP1 and others, (57-60)), are secreted (e.g. COBLL1 and others, (61-64)), or have been knocked out in mice, resulting in metabolic phenotypes (**Figure 7B**, **Table 3**, (65)).

Comparing Ca^{2+} dynamics across strains and sex offers one approach for designing future experiments

In addition to the candidate regulators with potential relevance to human islet biology, we offer access to our data where others can determine whether their gene of interest may have roles in islet biology. As noted above, multiple inferences regarding the roles of specific pathways are possible via analysis of Ca^{2+} oscillations in islets (6, 7, 16, 18) and our protein correlations provide a resource to identify which parameter most closely relates to a Ca^{2+} trait of interest. Additionally, it highlights the relevant extreme strains for a given trait and for the gene, giving guidance regarding the best mouse strain in which to explore that gene's role (e.g. **Figure 7C**). Newer technologies in reproductive assistance, transgenesis, and gene editing, together with more accurate genome sequencing and single mutations conferring docility, are quickly making utilization of the wild-derived mice more practical (55, 56, 66-68). As many of the QTL identified in DO-based studies often have strong driver SNPs from the wild-derived strains, a further understanding of which experimental questions might be best addressed by use of these strains will be important.

Our lab and others have previously provided databases for querying the expression of genes as a function of diet (WD vs chow, (69, 70)) and background (e.g. BTBR and B6, (69, 70)), correlation and QTL scans in F2 intercrosses of these mice (71), and where these may align with QTL in our DO studies (13). Many of our candidates are strongly altered by diet and have strong correlations in the F2 data for certain clinical traits including insulin and glycemic parameters (71). Here, we provide the correlation data for islet proteins against multiple parameters describing islet Ca2+ responses between strains (DOI: https://doi.org/10.5061/dryad.j0zpc86jc). These will enable researchers to better identify proteins or parameters of interest as well as appropriate background strains with which to determine the functions of these proteins.

MATERIALS & METHODS:

Chemicals:

All general chemicals, amino acids, BSA, DMSO, glucose, gastric inhibitory polypeptide (GIP,G2269), cOmplete Mini EDTA-free Protease Inhibitor Cocktail Tablets (11836170001), and heat-inactivated FBS (12306C) were purchased from Sigma Aldrich. RPMI 1640 base medium (11-875-093), antibiotic–antimycotic solutions (15240112), NP-40 Alternative (492016), Fura Red Ca^{2+} imaging dye (F3020), DiR (D12731), and agarose (BP1356-500) were purchased from ThermoFisher. Glass-bottomed culture dishes were ordered from Mattek (P35G-0-14-C). Fura Red stocks were prepared at 5 mM concentrations in DMSO, aliquoted into light-shielded tubes, and stored at –20°C until day of use (5 μM final concentration). DiR was prepared in DMSO at 2 mg/ mL, aliquoted to light-shielded tubes, and stored at 4°C until use. All imaging solutions were prepared in a bicarbonate/HEPES-buffered imaging medium (formula in **Table 1**). Amino acids were prepared as 100× stock in the biocarbonate/HEPES-buffered imaging medium, aliquoted into 1.5 mL tubes, and frozen at –20°C until day of use. Aliquots of GIP stock were prepared at 100 μM in water and kept at -20°C until day of use.

Animals:

Animal care and experimental protocols were approved by the University of Wisconsin-Madison Animal Care and Use Committee. Most strains (B6, AJ, 129, NOD, PWK, and WSB) were bred in-house, although two strains (CAST and NZO) were purchased from Jackson Laboratory (Bar Harbor, ME). All mice were fed a high-fat, high-sucrose Western-style diet (WD, consisting of 44.6% kcal fat, 34% carbohydrate, and 17.3% protein) from Envigo Teklad (TD.08811) beginning at 4 weeks and continuing until sacrifice (aged ~19-20 weeks for all strains except the NZO males). The NZO males were sacrificed at 12 weeks of age owing to complications from severe diabetes. For each strain, 3-7 males and females from at least 2 litters were analyzed. Animals were sacrificed by cervical dislocation prior to islet isolation.

In vivo measurements:

Fasting blood glucose and insulin levels were measured in mice at 19 weeks of age, except for the NZO males which were measured at 12 weeks of age. Glucose was analyzed by the glucose oxidase method using a commercially available kit (TR15221, Thermo Fisher Scientific), and insulin was measured by radioimmunoassay (RIA; SRI-13K, Millipore).

Islet imaging:

Islets were isolated as previously described (72) and incubated in recovery medium (RPMI 1640, 11.1 mM glucose, 1% antibiotic/antimycotic, 10% FBS) overnight at 37°C and 5% CO_2. Islets were then incubated with Fura Red (5 μM in recovery medium) at 37°C for 45 minutes. Imaging dishes were created from glass-bottomed 10 cm^2 dishes that had been filled with agarose. A channel with a central well was cut into the agarose with expanded ports on either side of the well for inflow and outflow lines. Prior to loading the chambers were perfused with the initial imaging solution (8 mM glucose in imaging medium). Islets were then loaded into these dishes. The imaging chamber was placed on a 37°C–heated microscope stage (Tokai Hit TIZ) of a Nikon A1R-Si+ confocal microscope. All solution reservoirs were kept in a 37°C water bath. Solutions were perfused through the chamber at 0.25 mL/min, with constant flow controlled by a Fluigent MCFS-EZ and M-switch valve assembly (Fluigent). The scope was integrated with a Nikon Eclipse-Ti Inverted scope and equipped with a Nikon CFI Apochromat Lambda D 10x/0.45 objective (Nikon Instruments), fluorescence spectral detector, and multiple laser lines (Nikon LU-NV laser unit; 405, 440, 488, 514, 561, 640nm). Bound dye was excited with the 405nm laser and the spectral detector's variable filter was set to 620-690nm. The free dye was excited with the 488nm laser and the variable filter collected from 640-690nm. Images were collected at 1 frame/sec at 6 second intervals. Each islet was considered a region of interest for further analysis. ROI intensity was collected by NIS Elements and exported for further analysis. All microscopy was

performed at the University of Wisconsin-Madison Biochemistry Optical Core, which was established with support from the University of Wisconsin-Madison Department of Biochemistry Endowment.

Islet perifusion:

Isolated islets were kept in RPMI-based medium (see above) overnight prior to perifusion, which was performed as previously described, with minor modifications (38, 73). Islets were equilibrated in 2 mM glucose for 55 minutes, after which 100 µL fractions were collected every minute with the perifusion solutions set at a flow rate of 100 µL/min. All solutions and islet chambers were kept at 37°C. After the final fraction was collected, islet chambers were disconnected, inverted, and flushed with 2 mL of NP-40 Alternative lysis buffer containing protease inhibitors for islet insulin extraction.

Secreted insulin assay:

Insulin in each perifusion fraction and islet insulin content were determined using a custom assay, as previously described (14).

Imaging data analysis:

Trace segments for each solution condition were analyzed using Matlab and R. Traces were detrended using custom R scripts and Graphpad PRISM. Custom Matlab scripts (https://github.com/hrfoster/Merrins-Lab-Matlab-Scripts, also stored on Dryad https://doi.org/10.5281/zenodo.6540721) determined oscillation peak amplitude, pulse duration, active duration (the time when Ca^{2+} is above 50% peak amplitude), silent duration (the difference between period and active duration). , plateau fraction (the fraction of overall time per pulse spent in the active duration), pulse period and other parameters. Spectral density deconvolution for the trace segments to determine principal frequencies was done using R. Animal averages for the different parameters defined by Matlab and R were computed and graphed using custom R scripts. Figures were created using CorelDraw and Biorender.com. All R scripts and the citations for the relevant packages used to generate them are available via Dryad (https://doi.org/10.5061/dryad.j0zpc86jc).

Correlation and Z-score calculations:

Correlation analysis was performed using the imaging data measurements and our published islet protein abundance data, *ex vivo* static insulin secretion measurements, and *in vivo* measurements made in a separate cohort of mice on the WD from the same strains and sexes used in these studies (14). For each imaging parameter or previously published measurement, the Z-score was calculated using the formula $z = (x-\mu) / \sigma$ where z is the Z-score, x is the animal average for that trait given the strain and sex, μ is the average of all animals' values for that trait, and σ is the standard deviation for all animals' values for that trait. Z-scores were computed in R and excel for the imaging parameters and the previously published (14) islet proteomic, *ex vivo* secretion, and *in vivo* measurements.

Correlation coefficients between the Z-score values of the imaging parameters and Z-scores of the previously published protein abundance, islet secretion, and *in vivo* traits were computed in Excel using the CORREL function. The equation used for this function is:

$$Correl(X,Y) = \frac{\sum(x-\dot{x})(y-\dot{y})}{\sum(x-\dot{x})^2 * \sum(y-\dot{y})^2}$$

Where X and Y are the Z-scores for the correlated traits/parameters, $\dot{x}$ is the population average for trait X and $\dot{y}$ is the population average for trait Y. Traits were considered highly correlated if absolute value for their Z-score correlation coefficients was ≥ 0.5.

Gene enrichment and human GWAS analysis:

Proteins highly correlated or anticorrelated to imaging parameters were further analyzed using pathway enrichment and presence of human GWAS SNPs. Briefly, for a given parameter, pathway analysis for the highly correlated or anti-correlated proteins to that parameter was done using Enrichr (74, 75).

For GWAS analysis, human orthologues for genes encoding the previously measured islet proteins were identified using BioMart (76). For highly correlated proteins, the protein was deemed of human interest if its orthologue had SNPs for glycemia-related traits (see table 2) either along the gene body,

within +/- 100 kbp of the gene start or end, or if any region in the gene body was connected to regions with SNPs by chromatin looping. SNPs were queried using Lunaris tool of the Common Metabolic Diseases Knowledge Portal (cmdkp.org). Chromatin loop anchor points for the relevant gene orthologues were identified using previously published human islet promoter-capture HiC data (35) and the alignment between these anchor loops and orthologues of interest was done using R scripts.

For those proteins having ortholgoues with SNPs via this analysis, we conducted further literature searches using Pubmed, Google Scholar, ChEMBL (59, 60, 77), canSAR (58), Uniprot (61), Tabula Muris (78), and the Human Protein Atlas (62, 63), and other resources (64, 79, 80) to determine tissue expression and identify any prior roles in islet biology. Figures for the relevant protein examples were created using Prism, CorelDraw, and the WashU Epigenome Browser (81).

Statistics:

For the islet perifusion insulin measurements, statistics were determined in GraphPad Prism. Fractional secretion area-under-the-curve (AUC) was determined using Prism and differences in AUCs analyzed using post-tests following 2-way ANOVA for the indicated trace segments. Islet total insulins between strains were compared using a two-tailed Student's t-test with Welch's correction.

Data Availability:

All R scripts and raw data are available via Dryad (https://doi.org/10.5061/dryad.j0zpc86jc). Image files are available upon request.

Study approval:

All protocols were approved by the University of Wisconsin-Madison IACUC (Protocol A005821-R01)

Author contributions. C. Emfinger, L. Clark, M. Merrins, M. Keller, and A. Attie designed experiments. C. Emfinger, L. Clark, K. Schueler, S. Simonett, D. Stapleton, and K. Mitok performed experiments. C. Emfinger and L. Clark wrote the paper. C. Emfinger, L. Clark, M. Keller performed data analysis. C. Emfinger, L. Clark, M. Merrins, M. Keller, and A. Attie edited the paper.

ACKNOWLEDGEMENTS:

Funding sources. This work was supported by NIH R01DK101573 to A. Attie, NIH R01DK113103 and VA I01B005113 to M. Merrins, and ADA 7-21-PDF-157 to C. Emfinger.

Portions of the figures were created with Biorender.com. License files are PC24P29AVO, UA24P29B1E, TK24P29B44, QM24P29H2P, WF24P29HB3, OM24P2BPIL, and BN24P2C01S.

REFERENCES:

1. Dimas AS, Lagou V, Barker A, Knowles JW, Mägi R, Hivert MF, et al. Impact of type 2 diabetes susceptibility variants on quantitative glycemic traits reveals mechanistic heterogeneity. *Diabetes.* 2014;63(6):2158-71.
2. Wood AR, Jonsson A, Jackson AU, Wang N, van Leewen N, Palmer ND, et al. A Genome-Wide Association Study of IVGTT-Based Measures of First-Phase Insulin Secretion Refines the Underlying Physiology of Type 2 Diabetes Variants. *Diabetes.* 2017;66(8):2296-309.
3. Clee SM, and Attie AD. The genetic landscape of type 2 diabetes in mice. *Endocr Rev.* 2007;28(1):48-83.
4. Kebede MA, and Attie AD. Insights into obesity and diabetes at the intersection of mouse and human genetics. *Trends in endocrinology and metabolism: TEM.* 2014;25(10):493-501.
5. Sittig LJ, Carbonetto P, Engel KA, Krauss KS, Barrios-Camacho CM, and Palmer AA. Genetic Background Limits Generalizability of Genotype-Phenotype Relationships. *Neuron.* 2016;91(6):1253-9.
6. Merrins MJ, Corkey BE, Kibbey RG, and Prentki M. Metabolic cycles and signals for insulin secretion. *Cell metabolism.* 2022;34(7):947-68.
7. Dahlgren GM, Kauri LM, and Kennedy RT. Substrate effects on oscillations in metabolism, calcium and secretion in single mouse islets of Langerhans. *Biochimica et biophysica acta.* 2005;1724(1-2):23-36.
8. Krippeit-Drews P, Düfer M, and Drews G. Parallel oscillations of intracellular calcium activity and mitochondrial membrane potential in mouse pancreatic B-cells. *Biochemical and biophysical research communications.* 2000;267(1):179-83.
9. Marinelli I, Thompson BM, Parekh VS, Fletcher PA, Gerardo-Giorda L, Sherman AS, et al. Oscillations in K(ATP) conductance drive slow calcium oscillations in pancreatic β-cells. *Biophys J.* 2022;121(8):1449-64.
10. Chen C, Chmelova H, Cohrs CM, Chouinard JA, Jahn SR, Stertmann J, et al. Alterations in β-Cell Calcium Dynamics and Efficacy Outweigh Islet Mass Adaptation in Compensation of Insulin Resistance and Prediabetes Onset. *Diabetes.* 2016;65(9):2676-85.
11. Threadgill DW, Miller DR, Churchill GA, and de Villena FP. The collaborative cross: a recombinant inbred mouse population for the systems genetic era. *Ilar J.* 2011;52(1):24-31.
12. Svenson KL, Gatti DM, Valdar W, Welsh CE, Cheng R, Chesler EJ, et al. High-resolution genetic mapping using the Mouse Diversity outbred population. *Genetics.* 2012;190(2):437-47.
13. Keller MP, Rabaglia ME, Schueler KL, Stapleton DS, Gatti DM, Vincent M, et al. Gene loci associated with insulin secretion in islets from nondiabetic mice. *The Journal of Clinical Investigation.* 2019;129(10):4419-32.
14. Mitok KA, Freiberger EC, Schueler KL, Rabaglia ME, Stapleton DS, Kwiecien NW, et al. Islet proteomics reveals genetic variation in dopamine production resulting in altered insulin secretion. *The Journal of biological chemistry.* 2018;293(16):5860-77.
15. Nunemaker CS, Wasserman DH, McGuinness OP, Sweet IR, Teague JC, and Satin LS. Insulin secretion in the conscious mouse is biphasic and pulsatile. *American Journal of Physiology-Endocrinology and Metabolism.* 2006;290(3):E523-E9.
16. Kennedy RT, Kauri LM, Dahlgren GM, and Jung SK. Metabolic oscillations in beta-cells. *Diabetes.* 2002;51 Suppl 1:S152-61.
17. Lang DA, Matthews DR, Peto J, and Turner RC. Cyclic oscillations of basal plasma glucose and insulin concentrations in human beings. *N Engl J Med.* 1979;301(19):1023-7.

18. Lewandowski SL, Cardone RL, Foster HR, Ho T, Potapenko E, Poudel C, et al. Pyruvate Kinase Controls Signal Strength in the Insulin Secretory Pathway. *Cell metabolism.* 2020;32(5):736-50.e5.
19. Colsoul B, Schraenen A, Lemaire K, Quintens R, Van Lommel L, Segal A, et al. Loss of high-frequency glucose-induced Ca2+ oscillations in pancreatic islets correlates with impaired glucose tolerance in Trpm5-/- mice. *Proceedings of the National Academy of Sciences of the United States of America.* 2010;107(11):5208-13.
20. Corbin KL, Waters CD, Shaffer BK, Verrilli GM, and Nunemaker CS. Islet Hypersensitivity to Glucose Is Associated With Disrupted Oscillations and Increased Impact of Proinflammatory Cytokines in Islets From Diabetes-Prone Male Mice. *Endocrinology.* 2016;157(5):1826-38.
21. Nunemaker CS, Bertram R, Sherman A, Tsaneva-Atanasova K, Daniel CR, and Satin LS. Glucose modulates [Ca2+]i oscillations in pancreatic islets via ionic and glycolytic mechanisms. *Biophys J.* 2006;91(6):2082-96.
22. Marinelli I, Parekh V, Fletcher P, Thompson B, Ren J, Tang X, et al. Slow oscillations persist in pancreatic beta cells lacking phosphofructokinase M. *Biophys J.* 2022;121(5):692-704.
23. Nunemaker CS, Zhang M, Wasserman DH, McGuinness OP, Powers AC, Bertram R, et al. Individual mice can be distinguished by the period of their islet calcium oscillations: is there an intrinsic islet period that is imprinted in vivo? *Diabetes.* 2005;54(12):3517-22.
24. Bertram R, Satin LS, and Sherman AS. Closing in on the Mechanisms of Pulsatile Insulin Secretion. *Diabetes.* 2018;67(3):351-9.
25. Fridlyand LE, Tamarina N, and Philipson LH. Bursting and calcium oscillations in pancreatic beta-cells: specific pacemakers for specific mechanisms. *American journal of physiology Endocrinology and metabolism.* 2010;299(4):E517-E32.
26. Whitticar NB, and Nunemaker CS. Reducing Glucokinase Activity to Enhance Insulin Secretion: A Counterintuitive Theory to Preserve Cellular Function and Glucose Homeostasis. *Frontiers in endocrinology.* 2020;11:378-.
27. Koneshamoorthy A, Seniveratne-Epa D, Calder G, Sawyer M, Kay TWH, Farrell S, et al. Case Report: Hypoglycemia Due to a Novel Activating Glucokinase Variant in an Adult - a Molecular Approach. *Front Endocrinol (Lausanne).* 2022;13:842937.
28. Tengholm A, and Gylfe E. cAMP signalling in insulin and glucagon secretion. *Diabetes, Obesity and Metabolism.* 2017;19(S1):42-53.
29. Shuai H, Xu Y, Ahooghalandari P, and Tengholm A. Glucose-induced cAMP elevation in β-cells involves amplification of constitutive and glucagon-activated GLP-1 receptor signalling. *Acta physiologica (Oxford, England).* 2021;231(4):e13611.
30. Koster JC, Marshall BA, Ensor N, Corbett JA, and Nichols CG. Targeted Overactivity of β Cell KATP Channels Induces Profound Neonatal Diabetes. *Cell.* 2000;100(6):645-54.
31. Remedi MS, and Nichols CG. In: Pitt GS ed. *Ion Channels in Health and Disease*. Boston: Academic Press; 2016:199-221.
32. Jennings RE, Scharfmann R, and Staels W. Transcription factors that shape the mammalian pancreas. *Diabetologia.* 2020;63(10):1974-80.
33. Rutter GA, Georgiadou E, Martinez-Sanchez A, and Pullen TJ. Metabolic and functional specialisations of the pancreatic beta cell: gene disallowance, mitochondrial metabolism and intercellular connectivity. *Diabetologia.* 2020;63(10):1990-8.
34. Stijnen P, Ramos-Molina B, O'Rahilly S, and Creemers JW. PCSK1 Mutations and Human Endocrinopathies: From Obesity to Gastrointestinal Disorders. *Endocr Rev.* 2016;37(4):347-71.
35. Miguel-Escalada I, Bonas-Guarch S, Cebola I, Ponsa-Cobas J, Mendieta-Esteban J, Atla G, et al. Human pancreatic islet three-dimensional chromatin architecture provides insights into the genetics of type 2 diabetes. *Nature genetics.* 2019.

36. Bergman RN, Zaccaro DJ, Watanabe RM, Haffner SM, Saad MF, Norris JM, et al. Minimal model-based insulin sensitivity has greater heritability and a different genetic basis than homeostasis model assessment or fasting insulin. *Diabetes.* 2003;52(8):2168-74.
37. Carter JD, Dula SB, Corbin KL, Wu R, and Nunemaker CS. A practical guide to rodent islet isolation and assessment. *Biol Proced Online.* 2009;11:3-31.
38. Emfinger CH, de Klerk E, Schueler KL, Rabaglia ME, Stapleton DS, Simonett SP, et al. β Cell–specific deletion of Zfp148 improves nutrient-stimulated β cell Ca2+ responses. *JCI Insight.* 2022;7(10).
39. Foster HR, Ho T, Potapenko E, Sdao SM, Lewandowski SL, VanDeusen HR, et al. Nutrient-dependent regulation of β-cell K_{ATP} channels is controlled by the isoforms of pyruvate kinase and the source of phosphoenolpyruvate. *bioRxiv.* 2022:2022.02.09.478817.
40. El K, Gray SM, Capozzi ME, Knuth ER, Jin E, Svendsen B, et al. GIP mediates the incretin effect and glucose tolerance by dual actions on α cells and β cells. *Sci Adv.* 2021;7(11).
41. Capozzi ME, Svendsen B, Encisco SE, Lewandowski SL, Martin MD, Lin H, et al. β Cell tone is defined by proglucagon peptides through cAMP signaling. *JCI Insight.* 2019;4(5).
42. Heart E, Corkey RF, Wikstrom JD, Shirihai OS, and Corkey BE. Glucose-dependent increase in mitochondrial membrane potential, but not cytoplasmic calcium, correlates with insulin secretion in single islet cells. *American Journal of Physiology-Endocrinology and Metabolism.* 2006;290(1):E143-E8.
43. Beck JA, Lloyd S, Hafezparast M, Lennon-Pierce M, Eppig JT, Festing MFW, et al. Genealogies of mouse inbred strains. *Nature genetics.* 2000;24(1):23-5.
44. Yang H, Wang JR, Didion JP, Buus RJ, Bell TA, Welsh CE, et al. Subspecific origin and haplotype diversity in the laboratory mouse. *Nature genetics.* 2011;43(7):648-55.
45. Lee KT, Karunakaran S, Ho MM, and Clee SM. PWD/PhJ and WSB/EiJ mice are resistant to diet-induced obesity but have abnormal insulin secretion. *Endocrinology.* 2011;152(8):3005-17.
46. Kreznar JH, Keller MP, Traeger LL, Rabaglia ME, Schueler KL, Stapleton DS, et al. Host Genotype and Gut Microbiome Modulate Insulin Secretion and Diet-Induced Metabolic Phenotypes. *Cell Reports.* 2017;18(7):1739-50.
47. Pearson JA, Wong FS, and Wen L. The importance of the Non Obese Diabetic (NOD) mouse model in autoimmune diabetes. *J Autoimmun.* 2016;66:76-88.
48. Andrikopoulos S, Fam BC, Holdsworth A, Visinoni S, Ruan Z, Stathopoulos M, et al. Identification of ABCC8 as a contributory gene to impaired early-phase insulin secretion in NZO mice. *The Journal of endocrinology.* 2016;228(1):61-73.
49. Ashcroft FM, Puljung MC, and Vedovato N. Neonatal Diabetes and the K_{ATP} Channel: From Mutation to Therapy. *Trends in Endocrinology & Metabolism.* 2017;28(5):377-87.
50. Pohorec V, Križančić Bombek L, Skelin Klemen M, Dolenšek J, and Stožer A. Glucose-Stimulated Calcium Dynamics in Beta Cells From Male C57BL/6J, C57BL/6N, and NMRI Mice: A Comparison of Activation, Activity, and Deactivation Properties in Tissue Slices. *Front Endocrinol (Lausanne).* 2022;13:867663.
51. Šterk M, Križančić Bombek L, Skelin Klemen M, Slak Rupnik M, Marhl M, Stožer A, et al. NMDA receptor inhibition increases, synchronizes, and stabilizes the collective pancreatic beta cell activity: Insights through multilayer network analysis. *PLoS computational biology.* 2021;17(5):e1009002.
52. Stožer A, Skelin Klemen M, Gosak M, Križančić Bombek L, Pohorec V, Slak Rupnik M, et al. Glucose-dependent activation, activity, and deactivation of beta cell networks in acute mouse pancreas tissue slices. *American journal of physiology Endocrinology and metabolism.* 2021;321(2):E305-e23.

53. Hauke S, Rada J, Tihanyi G, Schilling D, and Schultz C. ATP is an essential autocrine factor for pancreatic β-cell signaling and insulin secretion. *Physiol Rep.* 2022;10(1):e15159.
54. Scarl RT, Corbin KL, Vann NW, Smith HM, Satin LS, Sherman A, et al. Intact pancreatic islets and dispersed beta-cells both generate intracellular calcium oscillations but differ in their responsiveness to glucose. *Cell Calcium.* 2019;83:102081.
55. Hirose M, Hasegawa A, Mochida K, Matoba S, Hatanaka Y, Inoue K, et al. CRISPR/Cas9-mediated genome editing in wild-derived mice: generation of tamed wild-derived strains by mutation of the a (nonagouti) gene. *Scientific Reports.* 2017;7(1):42476.
56. Mochida K, Hasegawa A, Otaka N, Hama D, Furuya T, Yamaguchi M, et al. Devising Assisted Reproductive Technologies for Wild-Derived Strains of Mice: 37 Strains from Five Subspecies of Mus musculus. *PloS one.* 2014;9(12):e114305.
57. Stanford SM, Diaz MA, Ardecky RJ, Zou J, Roosild T, Holmes ZJ, et al. Discovery of Orally Bioavailable Purine-Based Inhibitors of the Low-Molecular-Weight Protein Tyrosine Phosphatase. *J Med Chem.* 2021;64(9):5645-53.
58. Coker EA, Mitsopoulos C, Tym JE, Komianou A, Kannas C, Di Micco P, et al. canSAR: update to the cancer translational research and drug discovery knowledgebase. *Nucleic acids research.* 2019;47(D1):D917-D22.
59. Davies M, Nowotka M, Papadatos G, Dedman N, Gaulton A, Atkinson F, et al. ChEMBL web services: streamlining access to drug discovery data and utilities. *Nucleic acids research.* 2015;43(W1):W612-W20.
60. Gaulton A, Hersey A, Nowotka M, Bento AP, Chambers J, Mendez D, et al. The ChEMBL database in 2017. *Nucleic acids research.* 2017;45(D1):D945-D54.
61. The UniProt C. UniProt: the universal protein knowledgebase in 2021. *Nucleic acids research.* 2021;49(D1):D480-D9.
62. Thul PJ, Åkesson L, Wiking M, Mahdessian D, Geladaki A, Ait Blal H, et al. A subcellular map of the human proteome. *Science (New York, NY).* 2017;356(6340).
63. Uhlén M, Fagerberg L, Hallström BM, Lindskog C, Oksvold P, Mardinoglu A, et al. Proteomics. Tissue-based map of the human proteome. *Science (New York, NY).* 2015;347(6220):1260419.
64. Uhlén M, Karlsson MJ, Hober A, Svensson AS, Scheffel J, Kotol D, et al. The human secretome. *Science signaling.* 2019;12(609).
65. Groza T, Gomez FL, Mashhadi HH, Muñoz-Fuentes V, Gunes O, Wilson R, et al. The International Mouse Phenotyping Consortium: comprehensive knockout phenotyping underpinning the study of human disease. *Nucleic acids research.* 2022:gkac972.
66. Karunakaran S, and Clee SM. Genetics of metabolic syndrome: potential clues from wild-derived inbred mouse strains. *Physiol Genomics.* 2018;50(1):35-51.
67. Chao T, Liu Z, Zhang Y, Zhang L, Huang R, He L, et al. Precise and Rapid Validation of Candidate Gene by Allele Specific Knockout With CRISPR/Cas9 in Wild Mice. *Frontiers in genetics.* 2019;10:124.
68. Chang PL, Kopania E, Keeble S, Sarver BAJ, Larson E, Orth A, et al. Whole exome sequencing of wild-derived inbred strains of mice improves power to link phenotype and genotype. *Mammalian genome : official journal of the International Mammalian Genome Society.* 2017;28(9-10):416-25.
69. Keller MP, Choi Y, Wang P, Davis DB, Rabaglia ME, Oler AT, et al. A gene expression network model of type 2 diabetes links cell cycle regulation in islets with diabetes susceptibility. *Genome research.* 2008;18(5):706-16.
70. Yau B, Naghiloo S, Diaz-Vegas A, Carr AV, Van Gerwen J, Needham EJ, et al. Proteomic pathways to metabolic disease and type 2 diabetes in the pancreatic islet. *iScience.* 2021;24(10):103099.

71. Lan H, Chen M, Flowers JB, Yandell BS, Stapleton DS, Mata CM, et al. Combined Expression Trait Correlations and Expression Quantitative Trait Locus Mapping. *PLOS Genetics.* 2006;2(1):e6.
72. Rabaglia ME, Gray-Keller MP, Frey BL, Shortreed MR, Smith LM, and Attie AD. α-Ketoisocaproate-induced hypersecretion of insulin by islets from diabetes-susceptible mice. *American Journal of Physiology-Endocrinology and Metabolism.* 2005;289(2):E218-E24.
73. Bhatnagar S, Oler AT, Rabaglia ME, Stapleton DS, Schueler KL, Truchan NA, et al. Positional cloning of a type 2 diabetes quantitative trait locus; tomosyn-2, a negative regulator of insulin secretion. *PLoS Genet.* 2011;7(10):e1002323.
74. Chen EY, Tan CM, Kou Y, Duan Q, Wang Z, Meirelles GV, et al. Enrichr: interactive and collaborative HTML5 gene list enrichment analysis tool. *BMC Bioinformatics.* 2013;14:128.
75. Kuleshov MV, Jones MR, Rouillard AD, Fernandez NF, Duan Q, Wang Z, et al. Enrichr: a comprehensive gene set enrichment analysis web server 2016 update. *Nucleic acids research.* 2016;44(W1):W90-7.
76. Smedley D, Haider S, Ballester B, Holland R, London D, Thorisson G, et al. BioMart--biological queries made easy. *BMC Genomics.* 2009;10:22.
77. Jupp S, Malone J, Bolleman J, Brandizi M, Davies M, Garcia L, et al. The EBI RDF platform: linked open data for the life sciences. *Bioinformatics.* 2014;30(9):1338-9.
78. Schaum N, Karkanias J, Neff NF, May AP, Quake SR, Wyss-Coray T, et al. Single-cell transcriptomics of 20 mouse organs creates a Tabula Muris. *Nature.* 2018;562(7727):367-72.
79. Varshney A, Scott LJ, Welch RP, Erdos MR, Chines PS, Narisu N, et al. Genetic regulatory signatures underlying islet gene expression and type 2 diabetes. *Proceedings of the National Academy of Sciences of the United States of America.* 2017;114(9):2301-6.
80. Lawlor N, George J, Bolisetty M, Kursawe R, Sun L, Sivakamasundari V, et al. Single-cell transcriptomes identify human islet cell signatures and reveal cell-type-specific expression changes in type 2 diabetes. *Genome research.* 2017;27(2):208-22.
81. Li D, Hsu S, Purushotham D, Sears RL, and Wang T. WashU Epigenome Browser update 2019. *Nucleic acids research.* 2019;47(W1):W158-W65.

FIGURES

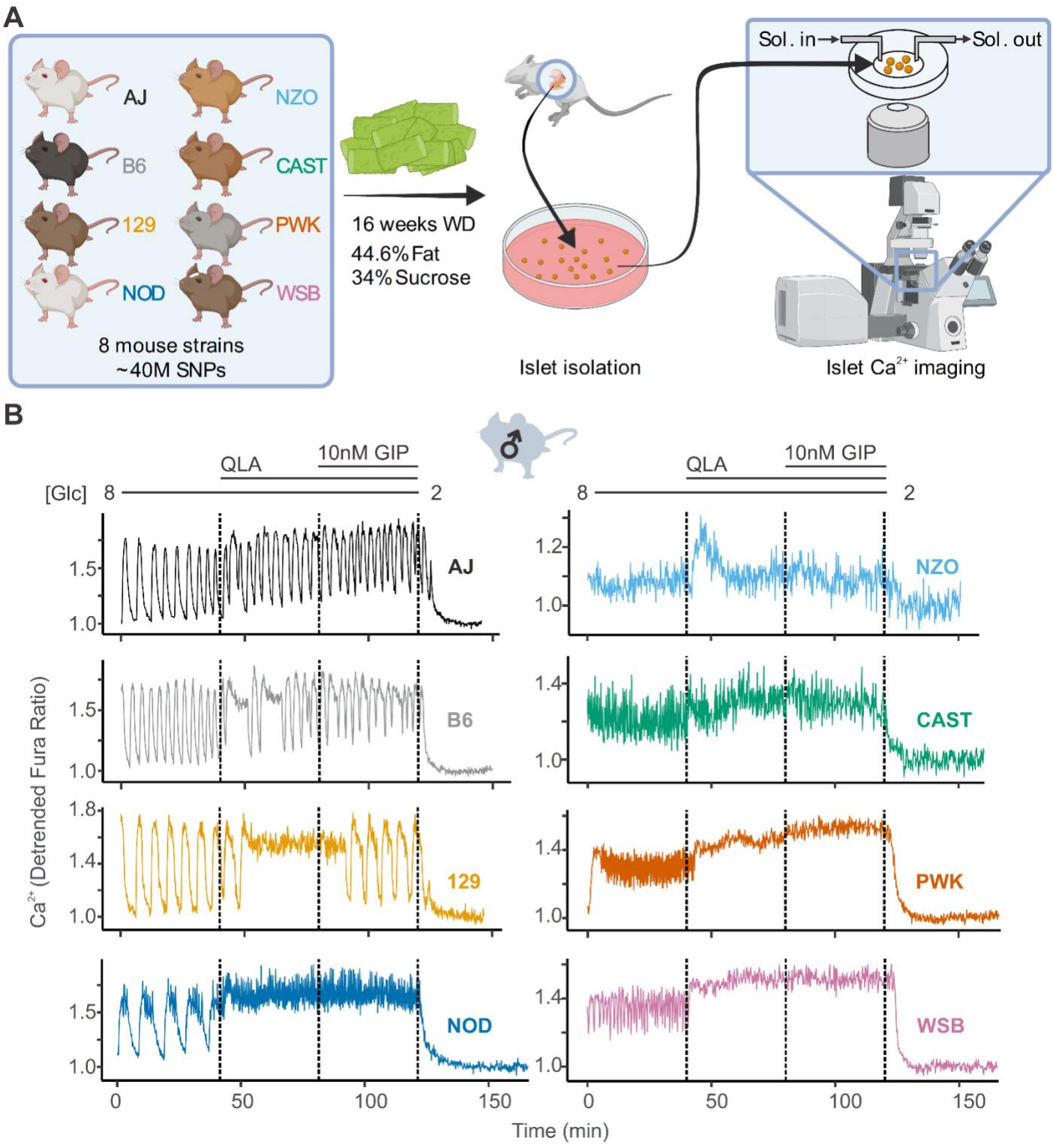

Figure 1. High diversity in Ca^{2+} oscillation across eight genetically distinct mouse strains.

(A) Male and female mice from eight strains (A/J; C57BL/6J (B6); 129S1/SvImJ (129); NOD/ShiLtJ

(NOD); NZO/HILtJ (NZO); CAST/EiJ (CAST); PWK/PhJ (PWK); and WSB/EiJ (WSB)) were placed on a Western Diet (WD) for 16 weeks, before their islets were isolated. The islets were then imaged on a confocal microscope using Fura Red dye under conditions of 8 mM glucose; 8 mM glucose + 2 mM L-glutamine, 0.5 mM L-leucine, and 1.25 nM L-alanine (QLA); 8 mM glucose + QLA + 10 nM GIP; and 2 mM glucose. **(B)** Representative Ca^{2+} traces for male mice (n = 3-8 mice per strain, and 15-83 islets per mouse), with the transitions between solution conditions indicated by dashed lines. Abbreviations: '[Glu]' = 'concentration of glucose in mM' ; 'Sol.' = 'solution'; 'SNPs'= 'single-nucleotide polymorphisms'

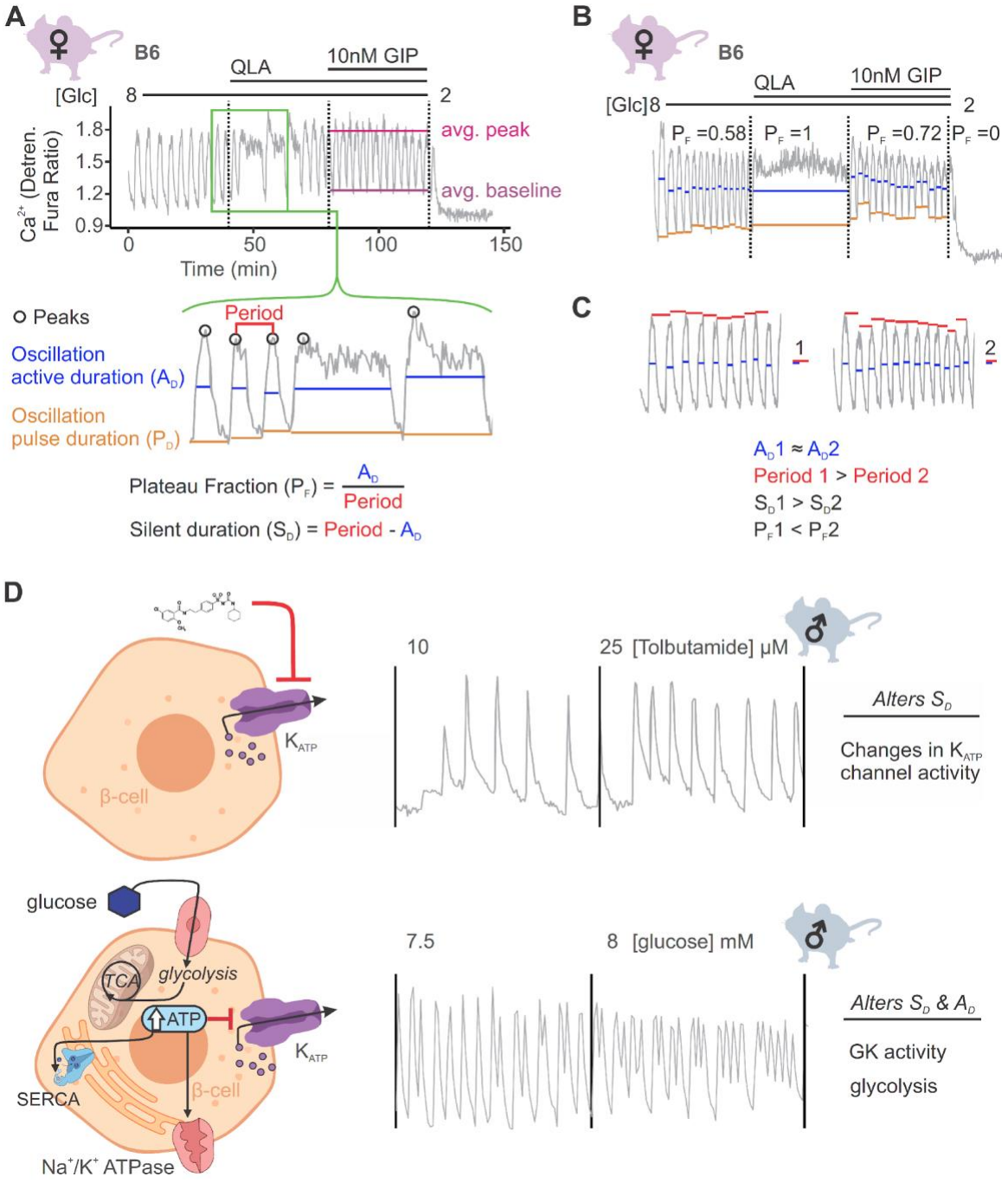

Figure 2. Ca^{2+} wave breakdown reveals mechanisms underlying Ca^{2+} responses. (A) In the example B6 female Ca^{2+} wave, the islet oscillations can change in their average peak and average baseline in response to different nutrients. Additionally, shifts in wave shape (green box) can be broken down into changes in time between peaks (period), the time in the active phase (active duration, A_D),

and the length of the oscillation (pulse duration, P_D). From these, the relative time in active phase, or plateau-fraction (P_F), and the time the islet is inactive between oscillations (silent duration, S_D) can be calculated. Each parameter can be changed by different underlying mechanisms. **(B)** For islets that plateaued, as in the example islet in 8/QLA, they were assigned a plateau-fraction of one and a period of zero. For islets that ceased to oscillate, such as the example islet in 2 mM glucose, they were assigned a plateau-fraction of zero and a period of the time of measurement (40 minutes). **(C)** For trace 1 (left), which has a longer period (red bars) than trace 2 (right), but the same active duration (blue bars), the silent duration is greater and consequently the P_F is shorter, in contrast to the trace in (**A**) where the P_F increases between 8mM and 8/QLA are largely due to increases in A_D. **(D)** Changes in specific Ca^{2+} wave parameters can reflect different mechanisms in β-cells. For example, changing K_{ATP} activity pharmacologically (upper panels) predominantly increases P_F by altering S_D, whereas increasing glucose concentrations by elevating glucose or activating GK cause significant alterations in both A_D and S_D to increase P_F. Abbreviations: '[Glc]' = 'concentration of glucose in mM' ; 'GK' = 'glucokinase'

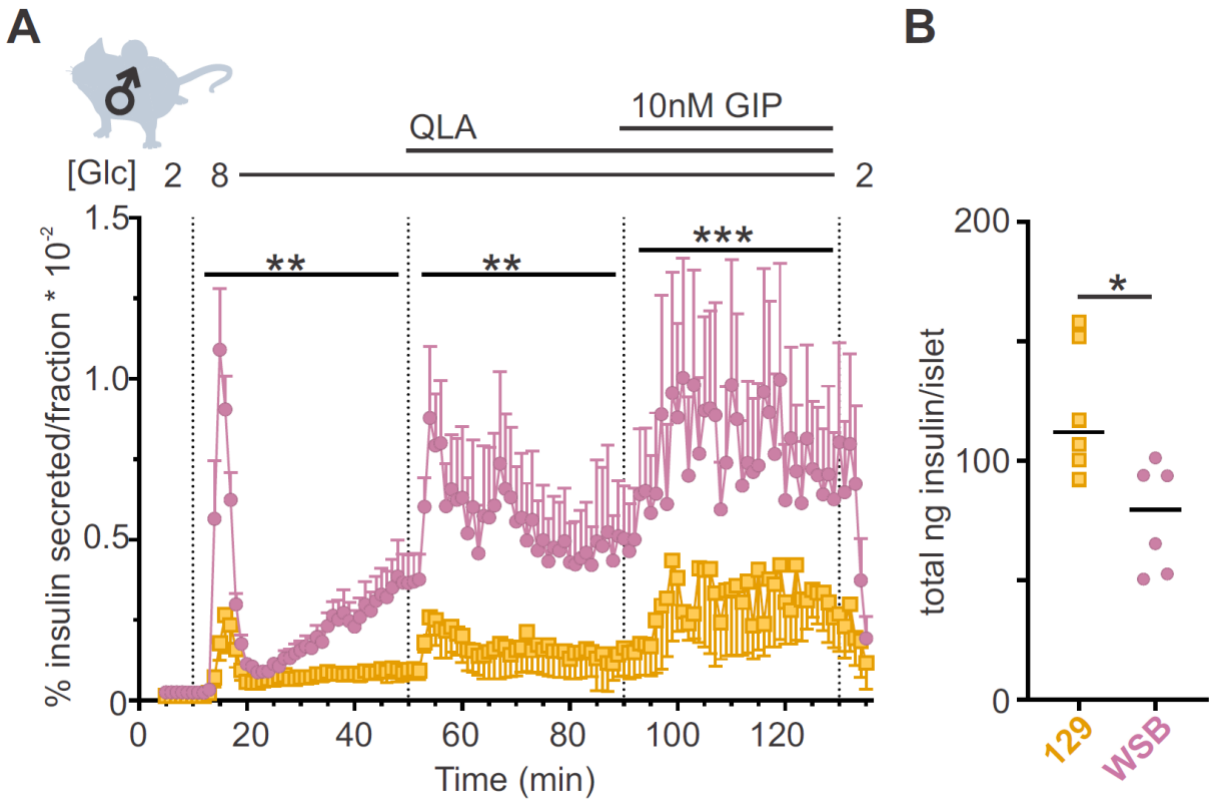

Figure 3. WSB mice secrete significantly more insulin than 129 mice. (**A**) Insulin secretion was measured for perifused islets from WSB (n=6, magenta circles) and 129 (n=5, yellow squares) male mice in 2 mM glucose, 8 mM glucose, 8 mM glucose + QLA, and 8 mM glucose + QLA + GIP. Transitions between solutions are indicated by dotted lines and the conditions for each are indicated above the graph. "[Glc]" denotes the concentration of glucose in mM. Data are shown as a percentage of total islet insulin (mean ± SEM). (**B**) Average total insulin per islet for the WSB and 129 males used in (**A**) with one exception: islets from one of the 129 mice were excluded from perifusion analysis due to technical issues with perifusion system on the day those animals' islets were perifused. Dots represent individual values, and the mean is denoted by the black line. For (**A**), asterisks denote strain effect for the area-und-the-curve of the section determined by 2-way ANOVA, mixed effects model; ** $p < 0.01$, *** $p < 0.001$. For (**B**), asterisk denotes $p < 0.05$ from Student's T-test with Welch's correction.

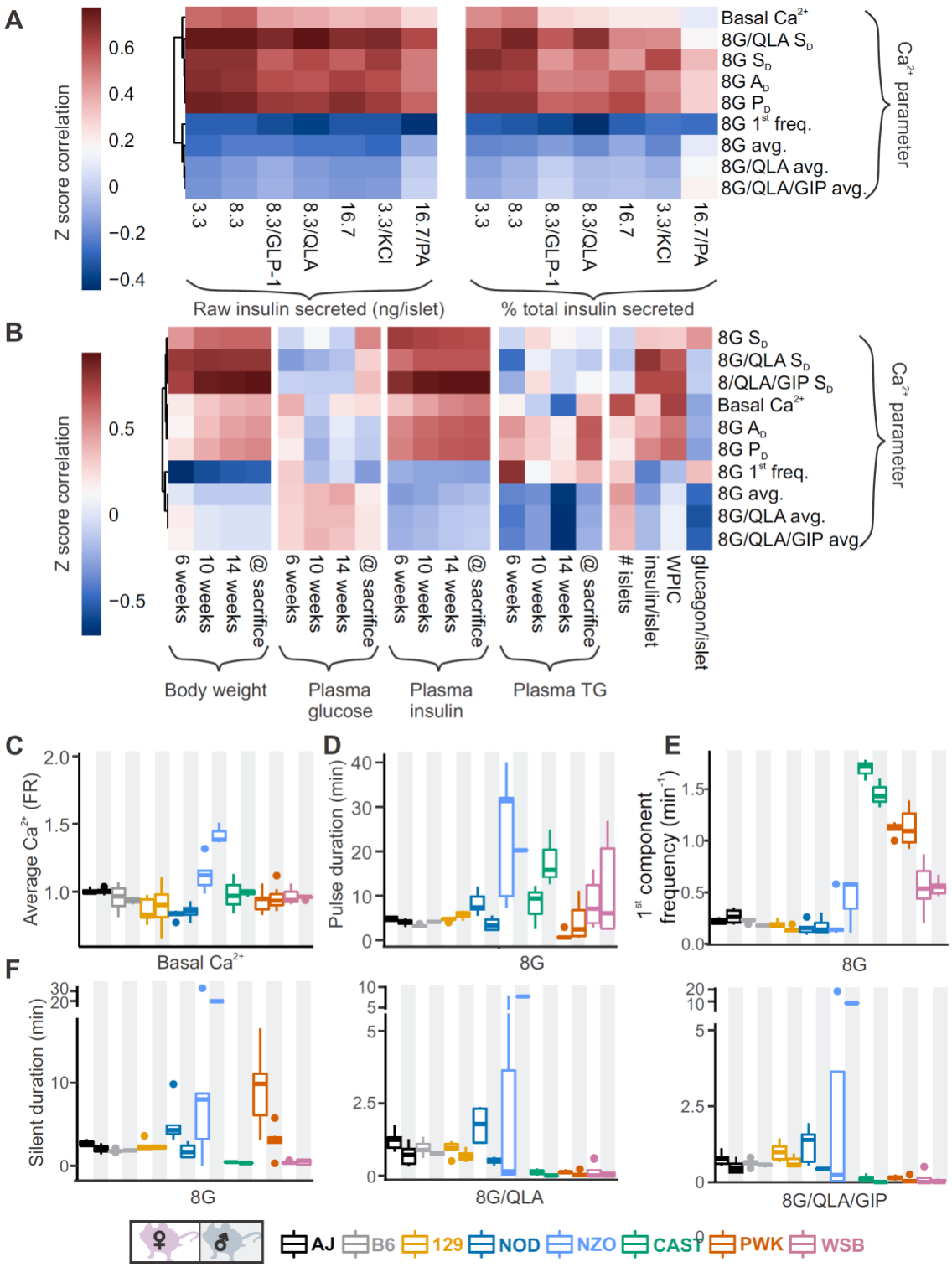

Figure 4. Comparing sex and strain patterns for Ca^{2+} metrics, insulin secretion, and clinical traits nominates Ca^{2+} metrics of interest. (A) The z-score correlation coefficient was calculated for

Ca^{2+} parameters and raw insulin secreted and % total insulin secreted. Insulin measurements were previously collected for seven different secretagogues (16.7 mM glucose + 0.5 mM palmitic acid (16.7G/PA); 3.3 mM glucose + 50 mM KCl (3.3G/KCl); 16.7 mM glucose (16.7G); 8.3 mM glucose + 1.25 mM L-alanine, 2 mM L-glutamine, and 0.5 mM L-leucine (8.3G/QLA); 8.3 mM glucose + 100 nM GLP-1 (8.3G/GLP-1); 8.3 mM glucose (8.3G); and 3.3 mM glucose (3.3G)) (32). (**B**) Correlation of the Ca^{2+} parameters to the clinical measurements in the founder mice which include 1) plasma insulin, triglycerides, and glucose at 6, 10, and 14 weeks as well as at time of sacrifice; 2) number of islets; 3) whole-pancreas insulin content (WPIC); and 5) islet content for insulin and glucagon. For (**A**) and (**B**), the Ca^{2+} parameters shown here include average Ca^{2+} in 2 mM glucose (basal Ca^{2+}); average Ca^{2+} in 8 mM glucose (8G avg.); average Ca^{2+} in 8 mM glucose + 1.25 mM L-alanine, 2 mM L-glutamine, and 0.5 mM L-leucine (8G/QLA avg); average Ca^{2+} in 8 mM glucose + QLA + 10 nM GIP (8G/QLA/GIP avg.); pulse duration in 8 mM glucose (8G P_D); active duration in 8G (8G A_D); silent duration in 8G (8G S_D), 8G/QLA (8G/QLA/S_D), and 8G/QLA/GIP (8G/QLA/GIP S_D); and 1st component frequency in 8 mM glucose (8G 1st freq.). Other parameters analyzed are indicated in supplemental figure 4. (**B-E**) Sex and strain variability for **(C)** average Ca^{2+} determined by the fura-ratio (FR) in 2 mM glucose, **(D)** pulse duration of oscillations in 8G, **(E)** 1st component frequency in 8G and **(F)** silent duration of oscillations in 8G, 8G/QLA, and 8G/QLA/GIP.

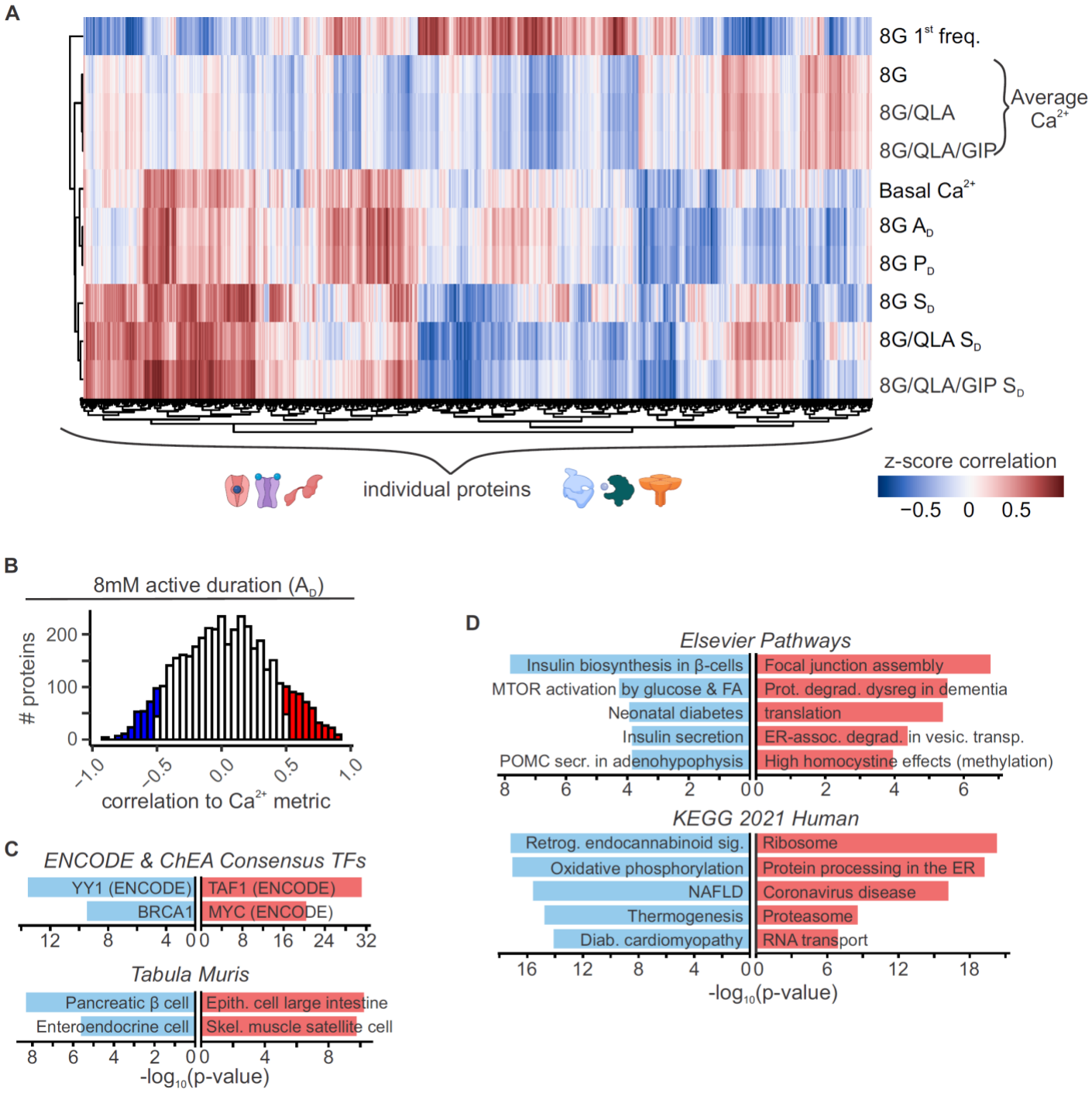

Figure 5. Islet proteins show correlation architecture to specific Ca^{2+} parameters. (**A**) Unsupervised clustering of correlation coefficients between protein abundance z-scores and z-scores for the Ca^{2+} parameters indicated. Islet proteins show differential correlation values to basal Ca^{2+}, excitatory Ca^{2+} (detrended average values for 8mM, 8/QLA, and 8/QLA/GIP), active duration and pulse

duration in 8mM glucose (8G P_D & A_D), and silent durations (S_D) in 8G, 8G/QLA, and 8G/QLA/GIP. Correlation coefficients for other parameters are indicated in Supplemental Figure 5. **(B)** Histograms representing the number of proteins that are correlated (red) and anti-correlated (blue) to 8G A_D. TRRUST transcription factor motif database and ARCHS4 Tissue signature database (C) as well as pathway enrichments for the Elsevier Pathway database and KEGG 2021 Human pathway database (D) (-$\log_{10}$(p-values)), for the highly correlated (red) and anticorrelated (blue) proteins to 8 A_D metric. Databases were queried using Enrichr (39, 40).

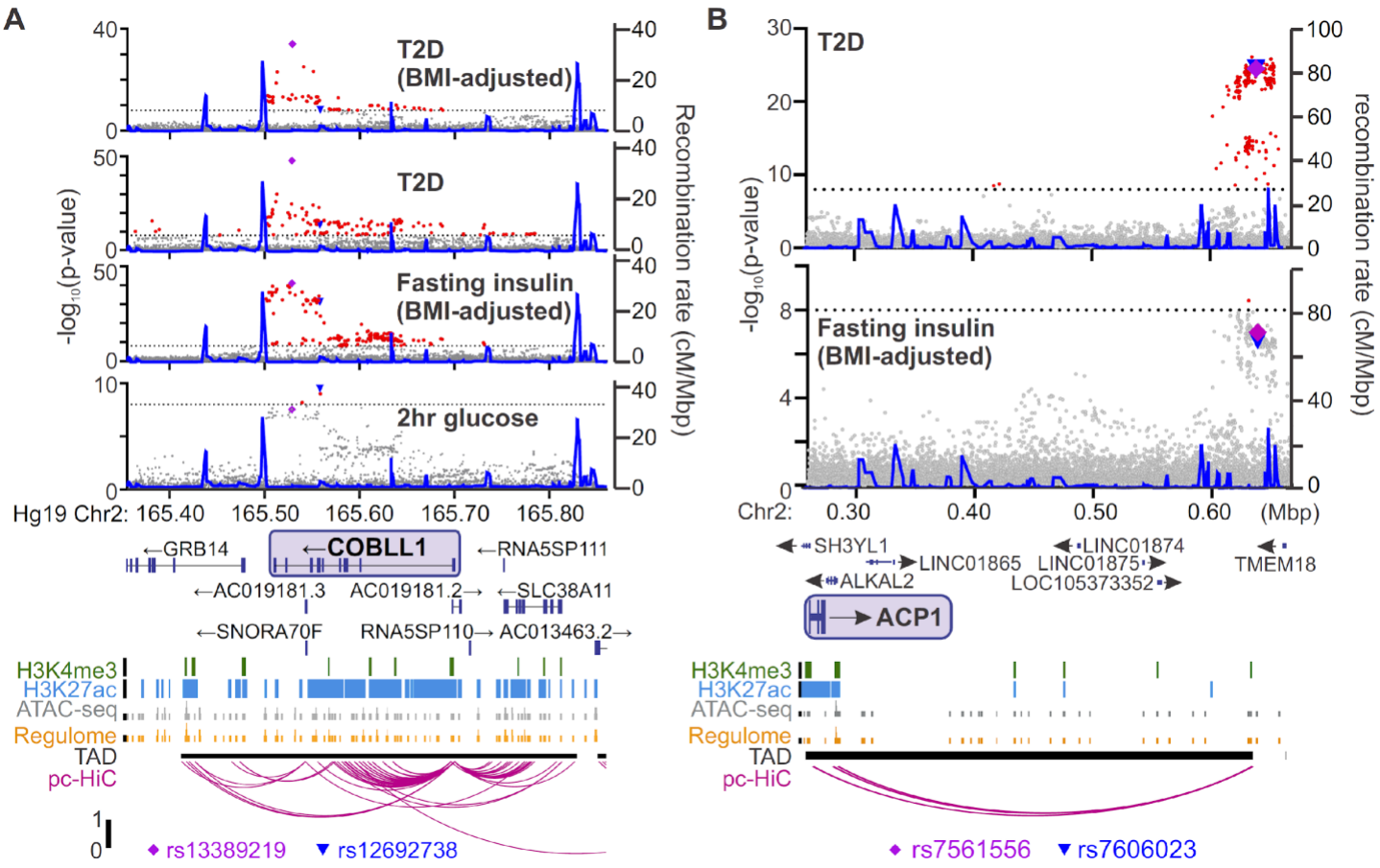

Figure 6. Identifying candidate protein targets by integrating human GWAS. (**A**) An example gene, *COBLL1*, orthologous to a gene coding for a protein identified as highly correlated to Ca^{2+} wave

parameters in the founder mice. The recombination rate is indicated by the solid blue line. Significant SNPs (8 < -$\log_{10}$(p), red) decorate the gene body for multiple glycemia-related parameters (in bold). Human islet chromatin data (34) for histone methylation, histone acetylation, ATAC-sequencing, and regulome score suggest active transcription of the gene. Human islet promoter-capture HiC data (34) show contacts between the SNP-containing regions decorating the gene and its promoter. The highest SNP for 2hr glucose (▾) and the other parameters (♦) are indicated. (**B**) Some orthologues did not show SNPs decorating the gene itself but did show looping to regions with SNPs for glycemic traits. The promoter of *ACP1*, for example, loops to a region within its topologically associated domain (black bar) with strong SNPs for type 2 diabetes risk and near-threshold SNPs for fasting insulin adjusted for BMI. Some SNPs (▾, ♦) lie directly on the contact regions identified by HiC, whereas others lie immediately proximal to these contacts. For both panels, the significance of association (-$\log_{10}$ of the p-value) for the individual SNPs is on the left y axis and the recombination rate per megabasepair is on the right y axis. Chromosomal position in Mbp is aligned to Hg19. SNP data were provided by the Common Metabolic Diseases Knowledge Portal (cmdkp.org).

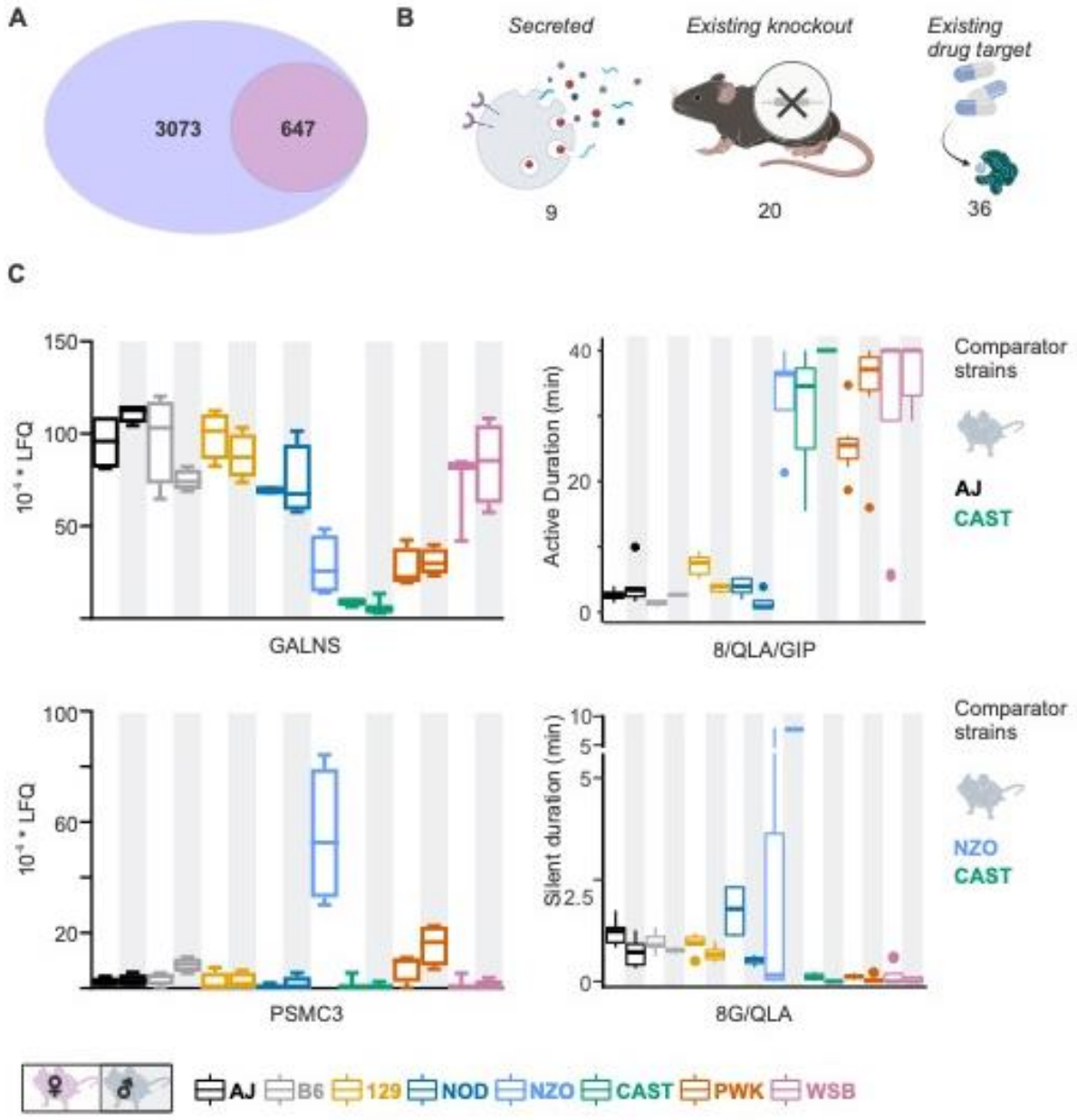

Figure 7. Strain variance alters model selections for protein/parameter testing. (**A**) Venn diagram illustrating that of 3073 proteins with significant correlation to at least 1 Ca^{2+} wave parameter of interest, 647 had orthologues with glycemic SNPs. (**B**) Of the 647 candidates, 9 were previously suggested to be secreted (61-64), 20 had existing KO mice with at least one metabolic phenotype (65), and 36 had existing compounds targeting them (57-60). (**C**) Example comparisons of strain variance

for proteins (left column, (4)) and Ca^{2+} traits (right column). GALNS (upper) is highly anticorrelated to several traits including active duration (A_D) in 8mM glucose + amino acids (8/QLA). Extreme strains to test the effect of gain or loss of this protein include B6 (high protein abundance and low A_D) and CAST (low protein abundance and high A_D), PSMC3 (lower) highly correlated to silent duration (S_D) for several conditions including 8mM glucose and QLA. The protein is largely absent in most strains (including AJ, which has low S_D) except the NZO, which has high S_D.

TABLES:

Component	**Concentration (mM)**
NaCl	137
KCl	5.6
$MgCl_2$	1.2
$NaH_2PO_4.H_2O$	0.5
$NaHCO_3$	4.2
HEPES	10
$CaCl_2$	2.6

Table 1: Imaging medium formula. Components are indicated by chemical abbreviation on the left and final concentration in mM is indicated in the right column.

Fasting hormones	Glucose-related	Tolerance test	Diabetes risk
insulin	fasting glucose	2hr glucose	T1D
proinsulin	random glucose	2hr insulin	T2D
c-peptide	Hba1c	2hr c-peptide	
fasting glc-BMI interaction		2hr insulin	
fasting ins-BMI interaction		Acute insulin response	
Gestational diabetes/altered fast glucose in pregnancy		SI-adjusted acute ins. Resp.	
		AUC insulin	
		AUC insulin/AUC glucose	
		Corrected insulin response	
		HOMA-B	
		HOMA-IR	
		Ins. Secretion rate	
		Ins. Sensitivity	
		Incremental ins. @ 30 min OGTT	
		Insulin @ 30min OGTT	
		Peak ins. response	
		Peak ins. Response adj SI	

Table 2 (on previous page): Categories included in SNP queries. These terms were considered as glycemia-related and are categorized as such on the Common Metabolic Diseases Knowledge portal, which was queried for the relevant SNPs. Also included but not listed here were variations of these terms that were adjusted for BMI.

Table 3 (on following pages): Proteins correlated with Ca^{2+} parameters that have glycemic-related SNPs. This includes protein IDs, gene names, gene IDs, and human orthologues for each of the proteins that correlate to one of the following metrics and have a glycemic-related SNP (see **Table 2**): basal Ca^{2+}, 8G S_D, 8G/QLA S_D, 8G/QLA/GIP S_D, 8G A_D, 8G P_D, and 8G 1^{st} freq.

Protein ID	Gene name	Gene ID or gene number	Human orthologue
Q9CQA1	Trappc5	66682	TRAPPC5
Q8CC86	Naprt	223646	NAPRT
Q5H8C4-2;Q5H8C4;Q8CDS8;Q6P6M9	Vps13a	271564	VPS13A
P10639	Txn	22166	TXN
I1E4X5;Q8BWQ6;D3YW20;D3YW19;Q8BWQ6-3	9030624J02Rik	71517	VPS35L
E0CXW2;E9PUK2;Q80V03-2;Q80V03	Adck5	268822	ADCK5
A2A6P4;Q8BKU4;Q9CQP1;Q3TYF6;Q3TY58	Fam104a	28081	FAM104A
Q91ZE0	Tmlhe	MGI:2180203	TMLHE
P70280	Vamp7	MGI:1096399	VAMP7
Q8VE95	C030006K11Rik	ENSMUSG00000116138	C8orf82
P42208;E9Q3V6;F6WYM0;D3YYB1;D3Z3C0	Septin2	ENSMUSG00000116048	SEPTIN2
Q543K9;P23492	Pnp	ENSMUSG00000115338	PNP
Q9CRC0	Vkorc1	ENSMUSG00000096145	VKORC1
Q6ZWR6-4;Q6ZWR6	Syne1	ENSMUSG00000096054	SYNE1
Q14A47;Q8K003	Tma7	ENSMUSG00000091537	TMA7
Q5BLJ7;P62301;Q921R2	Rps13	ENSMUSG00000090862	RPS13
Q9WV96;D6RG99;D3YVK5;D3YVK4	Timm10b	ENSMUSG00000089847	TIMM10B
Q9CPW2	Fdx2	ENSMUSG00000079677	FDX2
A0A087WQE6;A0A087WNT1;P83940;A0A087WPE4	Eloc	ENSMUSG00000079658	ELOC
Q8R2U0-2;Q8R2U0	Seh1l	ENSMUSG00000079614	SEH1L
Q9D002;Q9CZE1;Q545N1;P56873	Znrd2	ENSMUSG00000079478	ZNRD2
Q99JR8-2;Q99JR8;Q3TXH6;Q3TM59	Smarcd2	ENSMUSG00000078619	SMARCD2
S4R191;S4R1P3;S4R2T3;P0C8K7	Smim1	ENSMUSG00000078350	SMIM1
Q9JJQ6;Q3TLS9;Q8CCG9;Q00558	F8a	ENSMUSG00000078317	F8A1
Q80TA1;Q9D4D0	Selenoi	ENSMUSG00000075703	SELENOI
Q8VCQ3;E0CZ57	Nrbf2	ENSMUSG00000075000	NRBF2
Q3ULL5;Q99L45	Eif2s2	ENSMUSG00000074656	EIF2S2
G5E8V9;E9Q3G5	Arfip1	ENSMUSG00000074513	ARFIP1
Q9D9Z5	Dda1	ENSMUSG00000074247	DDA1
Q62084	Ppp1r14bl	ENSMUSG00000073730	PPP1R14B
O78207;W5XQG0;Q792Z7;P01899;Q31168;Q31167;O78206;O19467;Q569W0	H2-D1	ENSMUSG00000073411	HLA-E
B1AVZ0	Uprt	ENSMUSG00000073016	UPRT
P68369	Tuba1a	ENSMUSG00000072235	TUBA1A
Q505N7;Q3UW66;Q99J99	Mpst	ENSMUSG00000071711	MPST
Q3U781;Q9D6W4;P84104-2;P84104;A2A4X6	Srsf3	ENSMUSG00000071172	SRSF3
A2AP32;A2AP31;Q3UIU2	Ndufb6	ENSMUSG00000071014	NDUFB6
Q80X95	Rraga	ENSMUSG00000070934	RRAGA
Q9JJL8	Sars2	ENSMUSG00000070699	SARS2
Q04750	Top1	ENSMUSG00000070544	TOP1
Q544H0;Q9Z1D1;Q3THA0	Eif3g	ENSMUSG00000070319	EIF3G
Q8BTZ7	Gmppb	ENSMUSG00000070284	GMPPB
Q8BXR1;D3YY38	Slc7a14	ENSMUSG00000069072	SLC7A14
G3X9M0;Q9ER88;Q9ER88-2	Dap3	ENSMUSG00000068921	DAP3
Q3U7U8;C5H0E8;P62835;Q3V3W9;C5H0E9	Rap1a	ENSMUSG00000068798	RAP1A
Q9CQU1	Mfap1	ENSMUSG00000068479	MFAP1
D3YX27;Q3TXN0;Q3UJR3;Q9JIY5;S4R1B3;Q80V84;F6XUR8;F6TCV0;D3YX28	Htra2	ENSMUSG00000068329	HTRA2
Q8R0J7	Vps37b	ENSMUSG00000066278	VPS37B
Q9EPL8	Ipo7	ENSMUSG00000066232	IPO7
P11352	Gpx1	ENSMUSG00000063856	GPX1
Q6PAL3;Q8BNE3;Q8BSZ2	Ap3s2	ENSMUSG00000063801	AP3S2
Q9CQ65	Mtap	ENSMUSG00000062937	MTAP
Q4KL81;P63260;Q3TSB7;Q3UD81	Actg1	ENSMUSG00000062825	ACTG1
Q6P1A9;Q5EBG5;Q58ET1;Q80UT7;P12970	Rpl7a	ENSMUSG00000062647	RPL7A
Q9JME5	Ap3b2	ENSMUSG00000062444	AP3B2
Q3UIZ0;Q99KY4-2;Q99KY4;Q3UDE5	Gak	ENSMUSG00000062234	GAK
Q9DB29	Iah1	ENSMUSG00000062054	IAH1
Q3THU8;Q8VEM8;G5E902;Q3UB63;Q3U995	Slc25a3	ENSMUSG00000061904	SLC25A3
E9PVD1	Ccdc62	ENSMUSG00000061882	CCDC62
Q5M9L7;Q8BT90;P63276;Q3TK12	Rps17	ENSMUSG00000061787	RPS17
Q9CRY7	Gdpd1	ENSMUSG00000061666	GDPD1
A0MNP4;Q9ERF3;Q8BVQ0;D6RDC7	Wdr61	ENSMUSG00000061559	WDR61
Q6RJ37;Q5KTQ2;O35641;P01902;Q31634;Q31191;Q31148;Q31614;Q31290	H2-K1	ENSMUSG00000061232	HLA-E
Q9ER38	Tor3a	ENSMUSG00000060519	TOR3A
Q99L69;Q3U3J1;P50136	Bckdha	ENSMUSG00000060376	BCKDHA
G3UYD0;Q3UHU8;Q9ESZ8-5;Q9ESZ8-4;Q9ESZ8-3;Q9ESZ8-6;Q9ESZ8-2;Q9ESZ8	Gtf2i	ENSMUSG00000060261	GFT2I
Q9DCD8;Q58EV4;O70435;Q3TEL1;E0CX62	Psma3	ENSMUSG00000060073	PSMA3
P17156;B7U582	Hspa2	ENSMUSG00000059970	HSPA2
I6L960;G3X9Y5;Q6A0C5;E9Q735	Ube4a	ENSMUSG00000059890	UBE4A
Q4FZL1;Q5F2A7;P60843;Q3UXC2;Q3TGK7;Q3TFG3;Q3TLL6;Q3U8I0;Q78WR5	Eif4a1	ENSMUSG00000059796	EIF4A1
Q540I4;Q3TJS0;O08917;G3UYU4	Flot1	ENSMUSG00000059714	FLOT1
Q5NCJ9;Q8R1I1	Uqcr10	ENSMUSG00000059534	UQCR10
A2RSB1;B7ZNL2;Q8C1W9;Q78ZA7	Nap1l4	ENSMUSG00000059119	NAP1L4
Q642K1;Q58EW0;P35980;Q0QEW9;G3UZJ6;G3UZK4	Rpl18	ENSMUSG00000059070	RPL18
Q1WWK3;P43276	H1f5	ENSMUSG00000058773	H1-5
Q4PZA2-3;Q4PZA2-4;Q4PZA2;Q4PZA2-2	Ece1	ENSMUSG00000057530	ECE1
Q3UHJ0;Q3UHJ0-2	Aak1	ENSMUSG00000057230	AAK1
F6RPJ9;Q8CGB9;Q9JHR7	Ide	ENSMUSG00000056999	IDE
P42128	Foxk1	ENSMUSG00000056493	FOXK1
Q544Y7;P18760;F8WGL3;Q9CX22	Cfl1	ENSMUSG00000056201	CFL1
E9Q5W5;Q5SSH7-2;Q5SSH7	Zzef1	ENSMUSG00000055670	ZZEF1
A0AUN0;Q4G0C0;G3X928	Sec23ip	ENSMUSG00000055319	SEC23IP
Q8R395	Commd5	ENSMUSG00000055041	COMMD5
Q4W4C9;Q3TVC0;B2L107;P62761	Vsnl1	ENSMUSG00000054459	VSNL1
B0FTY3;Q8R1N4;Q8R1N4-2;Q8R1N4-3	Nudcd3	ENSMUSG00000053838	NUDCD3
Q61292;Q3USI2	Lamb2	ENSMUSG00000052911	LAMB2
Q9R1T2;Q9R1T2-2	Sae1	ENSMUSG00000052833	SAE1
Q7TMK6;Q3UWV9;Q3TKK8	Hook2	ENSMUSG00000052566	HOOK2
Q505D7	Opa3	ENSMUSG00000052214	OPA3
Q8K3W0;D3Z7P0;Q8K3W0-1;Q8K3W0-5;Q8K3W0-6;E9Q0U3;Q8K3W0-4	Babam2	ENSMUSG00000052139	BABAM2
Q9QY96;Q9QY96-2;Q8CDP3	Casr	ENSMUSG00000051980	CASR
A2ASS6;E9Q8N1;E9Q8K5;A2ASS6-2	Ttn	ENSMUSG00000051747	TTN
P43274	H1f4	ENSMUSG00000051627	H1-4
Q9CZP0	Ufsp1	ENSMUSG00000051502	UFSP1
Q91WK1	Spryd4	ENSMUSG00000051346	SPRYD4
Q9Z0W3;Q9Z0W3-2	Nup160	ENSMUSG00000051329	NUP160
Q2M4J2;Q9Z1B3-2;Q9Z1B3-3;Q9Z1B3;Q6ZQ92;Q3UPW0	Plcb1	ENSMUSG00000051177	PLCB1
A2AIL4	Ndufaf6	ENSMUSG00000050323	NDUFAF6
P27661	H2ax	ENSMUSG00000049932	H2AX
Q8R086	Suox	ENSMUSG00000049858	SUOX
P43275	H1f1	ENSMUSG00000049539	H1-1

Q3U3H9;P61963;Q80ZU1	Dcaf7	ENSMUSG00000049354	DCAF7
A2ASW4;Q9EQZ6-3;Q9EQZ6;A2ASW8;Q571A8;Q9EQZ6-2	Rapgef4	ENSMUSG00000049044	RAPGEF4
P59266	Fitm2	ENSMUSG00000048486	FITM2
O88845;Q3TR91;O88845-3	Akap10	ENSMUSG00000047804	AKAP10
Q3U487	Hectd3	ENSMUSG00000046861	HECTD3
Q566K0;P17095;Q3TE85	Hmga1	ENSMUSG00000046711	HMGA1
Q8C4B4;Q8C4B4-2	Unc119b	ENSMUSG00000046562	UNC119B
Q3UK83;Q3U7F3;Q3TIK8;Q5EBP8;P49312;Q3TFB1;P49312-2	Hnrnpa1	ENSMUSG00000046434	HNRNPA1
Q3UAP1;Q9WUQ2;D3Z3S1	Preb	ENSMUSG00000045302	PREB
Q4VAI2;Q9D358	Acp1	ENSMUSG00000044573	ACP1
Q8C298;E9Q179;Q8C5Q4	Grsf1	ENSMUSG00000044221	GRSF1
B2RX64;Q571E5;B7ZWH8	Prss53	ENSMUSG00000044139	PRSS53
Q8R3Y8-2;Q8R3Y8	Irf2bp1	ENSMUSG00000044030	IRF2BP1
P70399;P70399-3	Tp53bp1	ENSMUSG00000043909	TP53BP1
Q3TIU4	Pde12	ENSMUSG00000043702	PDE12
E9Q933;Q8BK08	Tmem11	ENSMUSG00000043284	TMEM11
Q52L87;P68373;Q3TIZ0	Tuba1c	ENSMUSG00000043091	TUBA1C
Q561M4;Q3UDC3;O88746	Tom1	ENSMUSG00000042870	TOM1
Q9JHC0	Gpx2	ENSMUSG00000042808	GPX2
D3Z7X0;D3Z2B3	Acad12	ENSMUSG00000042647	ACAD10
P70227	Itpr3	ENSMUSG00000042644	ITPR3
O70305-2;E9QM77;O70305;O70305-3;F6U2C2;Q3UX07;F7B6X4;Q3UX51	Atxn2	ENSMUSG00000042605	ATXN2
Q60520;Q60520-1	Sin3a	ENSMUSG00000042557	SIN3A
Q3TK27;Q8CI11;Q8CI11-2	Gnl3	ENSMUSG00000042354	GNL3
E9Q7L3;D3Z1W6;E9Q7L2;D3Z1N4;E9Q4Y5;F8VQD1;Q8BSQ9-2;Q8BSQ9;D3YYF2;D6RIL0;D6RI94;D3Z3R4;F6THL5	Pbrm1	ENSMUSG00000042323	PBRM1
Q3V3R4;Q3V391;Q05DI0	Itga1	ENSMUSG00000042284	ITGA1
Q3THL5;Q80X73	Pelo	ENSMUSG00000042275	PELO
B2RQR5;Q3TDT4;Q8BPQ7;D3Z7V4;D3YUT7	Sgsm1	ENSMUSG00000042216	SGSM1
E9Q481;Q6P2K6	Ppp4r3a	ENSMUSG00000041846	PPP4R3A
Q5SVI5;P52792;Q5SVI6;P52792-2	Gck	ENSMUSG00000041798	GCK
P12968	Iapp	ENSMUSG00000041681	IAPP
Q6V4S5	Sdk2	ENSMUSG00000041592	SDK2
Q8QZS1;E0CX19	Hibch	ENSMUSG00000041426	HIBCH
B2RVP5;Q3THW5;P0C0S6;Q8R029;Q3TFU6;Q3UA95	H2az2	ENSMUSG00000041126	H2AZ2
Q7TNG5;E9QK48;Q7TNG5-2;D3YWS2;D6RGM3	Eml2	ENSMUSG00000040811	EML2
Q8VDM6-2;Q8VDM6	Hnrnpul1	ENSMUSG00000040725	HNRNPUL1
E9QN47;Q80U28-14;A2AGQ7;A2AGR0;A2AGQ5;A2AGQ4;Q80U28-3;Q80U28-15;Q80U28;Q80U28-8;Q80U28-4;Q80U28-2;A6PWP8;Q80U28-13	Madd	ENSMUSG00000040687	MADD
E9Q9J4;Q6ZQB6-3;Q6ZQB6;Q6ZQB6-2;Q80V47	Ppip5k2	ENSMUSG00000040648	PPIP5K2
K3W4R5;A2AGT5-3;A2AGT5;Z4YL78;A2AGT5-2;Q80U79	Ckap5	ENSMUSG00000040549	CKAP5
Q8K4R4-2;X1WI19;Q8BTD8;Q8K4R4-3;Q8K4R4;Q8K4R4-4	Pitpnc1	ENSMUSG00000040430	PITPNC1
A2AFS3	Elapor1	ENSMUSG00000040412	ELAPOR1
Q6NZR5;Q3TW36;Q8CDP6;O70349;Q8R3X0;Q3TE28	Skiv2l	ENSMUSG00000040356	SKIV2L
S4R2J9;Q3TLH4-5;Q3TLH4;S4R294	Prrc2c	ENSMUSG00000040225	PRRC2C
B2RUS7;Q8BNE2;Q6PGE2;Q9Z2P1	Abcc8	ENSMUSG00000040136	ABCC8
Q91YT7;Q3UNH5	Ythdf2	ENSMUSG00000040025	YTHDF2
Q542C3;P59114	Pcif1	ENSMUSG00000039849	PCIF1
Q5U458;E9Q8B3	Dnajc11	ENSMUSG00000039768	DNAJC11
P60670;Q3UE06;Q3UDU9;P60670-2	Nploc4	ENSMUSG00000039703	NPLOC4
Q543N6;P58389;Q8C0E1;A2AWE9;A2AWF0	Ptpa	ENSMUSG00000039515	PTPA
Q8R0G9;Q8CDZ5	Nup133	ENSMUSG00000039509	NUP133
Q80UI9;Q3TDI2;P56695;Q3UN10	Wfs1	ENSMUSG00000039474	WFS1
Q91X52;A2AC16	Dcxr	ENSMUSG00000039450	DCXR
G3X972;Q80U83;Q3V222;Q8R2V9	Sec24c	ENSMUSG00000039367	SEC24C
Q9QXV0	Pcsk1n	ENSMUSG00000039278	PCSK1N
Q3UD03;Q3U199;Q3TCV9;Q6NSR8	Npepl1	ENSMUSG00000039263	NPEPL1
E9QLB2;Q3UFF7	Lyplal1	ENSMUSG00000039246	LYPLAL1
Q8BYA0	Tbcd	ENSMUSG00000039230	TBCD
Q9Z2H7	Gipc2	ENSMUSG00000039131	GIPC2
P97449;Q3UP74;Q3TB69	Anpep	ENSMUSG00000039062	ANPEP
Q9D0A3	Arpin	ENSMUSG00000039043	ARPIN-AP3S2
Q9WVJ3-2;Q9WVJ3;Q3U496	Cpq	ENSMUSG00000039007	CPQ
Q8C1L7;Q9CQR2	Rps21	ENSMUSG00000039001	RPS21
Q80U95	Ube3c	ENSMUSG00000039000	UBE3C
Q8C9B9	Dido1	ENSMUSG00000038914	DIDO1
Q5BLK0;P35979;Q8C2K0;Q3TIQ2	Rpl12	ENSMUSG00000038900	RPL12
E9Q8A3;Q8BKC8-2;Q8BKC8;Q8BKC8-3	Pi4kb	ENSMUSG00000038861	PI4KB
Q8BM55;D3Z6S1;Q8BM55-3;Q8BM55-2	Tmem214	ENSMUSG00000038828	TMEM214
Q5RL55;Q6P542	Abcf1	ENSMUSG00000038762	ABCF1
B7ZMR0;Q76LS9-2;Q76LS9	Mindy1	ENSMUSG00000038712	MINDY1
P56135;F8WHP8	Atp5j2	ENSMUSG00000038690	ATP5MF
Q8BXL7;E9PZK7	Arfrp1	ENSMUSG00000038671	ARFRP1
P60840-2;P60840;P60840-3	Ensa	ENSMUSG00000038619	ENSA
Q9JIS5	Sv2a	ENSMUSG00000038486	SV2A
Q80U12;Q80U12-2	Sgsm2	ENSMUSG00000038351	SGSM2
Q8BJT9;Q8BJR2;Q91VV3;Q8BK85	Edem2	ENSMUSG00000038312	EDEM2
Q9D7E3	Ovca2	ENSMUSG00000038268	OVCA2
B2RXC1	Trappc11	ENSMUSG00000038102	TRAPPC11
Q8VDN4;D3YUR9	Ccdc92	ENSMUSG00000037979	CCDC92
Q5F2E7;Q5F2E7-2	Nufip2	ENSMUSG00000037857	NUFIP2
Q3U7P6;Q05915;Q3UC70	Gch1	ENSMUSG00000037580	GCH1
Q922B3;Q3UDC5	Icam1	ENSMUSG00000037405	ICAM1
O88712-2;O88712;O88712-3	Ctbp1	ENSMUSG00000037373	CTBP1
Q99MR6-3;Q99MR6-4;Q99MR6-2;Q99MR6	Srrt	ENSMUSG00000037364	SRRT
E9Q0R0;B1ATV4;Q3V165;B1ATV6;B1ATV5;Q8K2G4-2;Q8K2G4	Bbs7	ENSMUSG00000037325	BBS7
Q543N5;Q9QYB1	Clic4	ENSMUSG00000037242	CLIC4
Q6GQU1;Q3UPC4;Q3TJE3;P17710-3;Q3UE51;G3UVV4;P17710-4;P17710;P17710-2;Q3TTB4	Hk1	ENSMUSG00000037012	HK1
B2RRE7	Otud4	ENSMUSG00000036990	OTUD4
Q8BQ47;D3Z0T5	Cnpy4	ENSMUSG00000036968	CNPY4
Q6ZPU9;H3BIY2;E0CXJ9;Q6ZPU9-2	Kifbp	ENSMUSG00000036955	KIFBP
B1AU25;Q9Z0X1;Q2QKE3	Aifm1	ENSMUSG00000036932	AIFM1
P68372;Q9CVR0;Q9DCR1	Tubb4b	ENSMUSG00000036752	TUBB4B
Q8CJG0;Q8CGT9;Q6P239;Q8R3Q7;Q6PHA2	Ago2	ENSMUSG00000036698	AGO2
Q923C1;A2AJ15;Q8BTW7	Man1b1	ENSMUSG00000036646	MAN1B1
Q6RUT9;O70496;Q8CCI9;E9PYL4	Clcn7	ENSMUSG00000036636	CLCN7
Q9CTE8;Q9DB25	Alg5	ENSMUSG00000036632	ALG5
Q8K1L5	Ppp1r11	ENSMUSG00000036398	PPP1R11
Q6ZWZ2	Ube2r2	ENSMUSG00000036241	UBE2R2
Q9ERS2	Ndufa13	ENSMUSG00000036199	NDUFA13
Q5SZA3;P15864	H1f2	ENSMUSG00000036181	H1-2
E9QMN5;Q8CHY6	Gatad2a	ENSMUSG00000036180	GATAD2A
Q6P5C5;Q3T9H8	Smug1	ENSMUSG00000036061	SMUG1

Q6PB44-2;Q6PB44	Ptpn23	ENSMUSG00000036057	PTPN23
Q8C0L8	Cog5	ENSMUSG00000035933	COG5
Q545I7;P01325	Ins1	ENSMUSG00000035804	INS
B2RRC5;A2AWA9	Rabgap1	ENSMUSG00000035437	RABGAP1
A1ILG8;Q8BX70;Q8BX70-3;Q8BX70-2	Vps13c	ENSMUSG00000035284	VPS13C
Q3U896;Q9Z2D0	Mtmr9	ENSMUSG00000035078	MTMR9
Q3UMF0-3;B1AZ15;B1AZ14;Q3UMF0-4;Q3UMF0-2;Q3UMF0	Cobll1	ENSMUSG00000034903	COBLL1
Q8K133;Q0PD31;P35290	Rab24	ENSMUSG00000034789	RAB24
Q3TRK3;Q9QXS6-3;Q9QXS6;Q9QXS6-2	Dbn1	ENSMUSG00000034675	DBN1
I7HPW8;F6YB52	Myo15b	ENSMUSG00000034427	MYO15B
Q9CV53;Q91WK5	Gcsh	ENSMUSG00000034424	GCSH
Q3UXQ1;Q05CG5;O55176;B1AXU3;B1AXU4;O55176-5;O55176-4;O55176-2	Pja1	ENSMUSG00000034403	PJA1
Q9D486-3;Q9D486;B2RY70;Q9D486-2	Cmip	ENSMUSG00000034390	CMIP
Q5SVF7;O55125;Q3UGS1;Q5SVG6	Nipsnap1	ENSMUSG00000034285	NIPSNAP1
Q8R3P6;Q8R3P6-2	Ints14	ENSMUSG00000034263	INTS14
P46460	Nsf	ENSMUSG00000034187	NSF
Q8K3X4	Irf2bpl	ENSMUSG00000034168	IRF2BPL
E9PU87;F6S7W6;Q6P4S6;F6U6U5;F6U8X4;Q6P4S6-2	Sik3	ENSMUSG00000034135	SIK3
Q8R3G9	Tspan8	ENSMUSG00000034127	TSPAN8
B9EKJ7;P58871;Z4YJL4	Tnks1bp1	ENSMUSG00000033955	TNKS1BP1
Q8K2C9	Hacd3	ENSMUSG00000033629	HACD3
Q6A0A2;Q6A0A2-2;Q6A0A2-3	Larp4b	ENSMUSG00000033499	LARP4B
Q8K2I1;D3YWJ4	Fntb	ENSMUSG00000033373	CHURC1-FNTB
Q8BFW7;Q8BFW7-4;Q8BFW7-5	Lpp	ENSMUSG00000033306	LPP
Q5EBQ2;P70296;Q3TGC5;D3Z1V4;D6RHS6	Pebp1	ENSMUSG00000032959	PEBP1
Q7TQH0-2;Q7TQH0-3;Q7TQH0;Q3TGG2;E9Q5Q0;Q3TYH7	Atxn2l	ENSMUSG00000032637	ATXN2L
Q921M8;Q3TEX8;P35123;Q6NXV6;Q5DTK8;Q3TPN5	Usp4	ENSMUSG00000032612	USP4
Q8BML9;Q8BU21;Q3TN94;D3Z158;Q3TIN2;Q8R1V9	Qars	ENSMUSG00000032604	QARS1
Q8K1M3;P12367	Prkar2a	ENSMUSG00000032601	PRKAR2A
Q8R146-2;Q8R146	Apeh	ENSMUSG00000032590	APEH
Q5DTS4;S4R1W5;Q8R388;O88720;Q3ULB0	Rbm6	ENSMUSG00000032582	RBM6
Q4VA21;Q3TQM5;Q8BH16	Fbxl2	ENSMUSG00000032507	FBXL2
P27546-2;P27546;P27546-3;E9PZ43	Map4	ENSMUSG00000032479	MAP4
Q80YA7	Dpp8	ENSMUSG00000032393	DPP8
Q8BHI7;D3Z0Z6;D3Z136	Elovl5	ENSMUSG00000032349	ELOVL5
Q3TE95;Q8BP92	Rcn2	ENSMUSG00000032320	RCN2
P41241;Q3UVH2;Q8BIS9	Csk	ENSMUSG00000032312	CSK
F8WIE1;Q8BWY6;Q3ZCX9;Q91W89;E9PZ88;Q3TBQ3;E9PYM7	Man2c1	ENSMUSG00000032295	MAN2C1
Q2M4G8;O35239	Ptpn9	ENSMUSG00000032290	PTPN9
G3X915;Q9D7V2	Lysmd2	ENSMUSG00000032184	LYSMD2
Q99L41;Q3UPG1;Q3UBC6;P22907-2;P22907	Hmbs	ENSMUSG00000032126	HMBS
Q80X80;Q8CAA2;Q3U590;Q9DBJ2;Q6PHC0;Q80U48;Q8CFV7	C2cd2l	ENSMUSG00000032120	C2CD2L
F8WIG4;Q3TI08;Q3TY03;Q62384;F8WHU9;Q9JJA1;Q3TIH8;Q9CUE2;Q8C8U3	Zpr1	ENSMUSG00000032078	ZPR1
Q8VEB4	Pla2g15	ENSMUSG00000031903	PLA2G15
Q8R1U1;G3UWH9;Q7TSQ9	Cog4	ENSMUSG00000031753	COG4
Q8CBB7;Q3UKX8;P22892;Q8CC03	Ap1g1	ENSMUSG00000031731	AP1G1
Q8BHC2;Q9CX00	Ist1	ENSMUSG00000031729	IST1
Q99LG2;Q3U316;E9PV58;Q3U1S0	Tnpo2	ENSMUSG00000031691	TNPO2
Q3UTJ2	Sorbs2	ENSMUSG00000031626	SORBS2
P18581-2;E9QJY0;P18581	Slc7a2	ENSMUSG00000031596	SLC7A2
Q78P93;Q3U646;Q9WV54;Q3U8A7;Q3TWT5	Asah1	ENSMUSG00000031591	ASAH1
Q61733	Mrps31	ENSMUSG00000031533	MRPS31
E9PXE2;Q3UHQ9;G3UX72;E9PXE1;Q6PDM6;D3YUF3;D3YUF4;G3UXP9;E9Q863;E9PY13;E9PY12;E9QPM7;Q003U3;Q64096;G3UYM8;Q80U26;F6VR53	Mcf2l	ENSMUSG00000031442	MCF2L
Q499D4;Q3TM67;Q9ESX5;Q3TI79;B7ZCL7;F6YUI5	Dkc1	ENSMUSG00000031403	DKC1
B7ZCL8;Q542P4;P70290;Q684Q6;A2AN84;B7ZCL9	Mpp1	ENSMUSG00000031402	MPP1
I7HPY1;I7HLV5;Q9D8T0;I7HJS7;J3JS95	Fam3a	ENSMUSG00000031399	FAM3A
Q9Z2D6-2;Q9Z2D6	Mecp2	ENSMUSG00000031393	MECP2
Q684Q8;B1AUY7;Q540H0;Q9QY36;B1AUY8;B1AUY9;B1AUZ1	Naa10	ENSMUSG00000031388	NAA10
Q61191;B1AUX2	Hcfc1	ENSMUSG00000031386	HCFC1
B9EKP5;B7FAU9;Q8BTM8;B7FAV1;Q6KAM8	Flna	ENSMUSG00000031328	FLNA
A2AQW0	Map3k15	ENSMUSG00000031303	MAP3K15
Q3UFJ3;P35486	Pdha1	ENSMUSG00000031299	PDHA1
Q0PD14;Q8BHC1	Rab39b	ENSMUSG00000031202	RAB39B
P46737;P46737-2	Brcc3	ENSMUSG00000031201	BRCC3
Q9D6K8	Fundc2	ENSMUSG00000031198	FUNDC2
A3KMJ8;P61759;Q3TIR6	Vbp1	ENSMUSG00000031197	VBP1
Q6A028	Swap70	ENSMUSG00000031015	SWAP70
A0A067XG53;B9EJ23;B7ZP42;O70589-3;O70589-4;O70589-5;O70589;O70589-2	Cask	ENSMUSG00000031012	CASK
Q0VDQ3;Q9D733;Q9D6X7	Gp2	ENSMUSG00000030954	GP2
P70452	Stx4a	ENSMUSG00000030805	STX4
Q91W34;D6RDS0;Q91W34-2	Rusf1	ENSMUSG00000030780	RUSF1
Q9JIF7	Copb1	ENSMUSG00000030754	COPB1
Q3TS44;Q9R1P4	Psma1	ENSMUSG00000030751	PSMA1
Q8R1B4;Q66JU1	Eif3c	ENSMUSG00000030738	EIF3CL
Q91WG2;Q91WG2-2;Q91WG2-1;Q3TZJ2	Rabep2	ENSMUSG00000030727	RABEP2
Q3U232;Q3U1N0;O89053;Q3U9K3;Q3T9L1;G3UYK8	Coro1a	ENSMUSG00000030707	CORO1A
Q0VG22;Q9JMD3;Q52LA1;E9PVP0;Q5RL65;Q6PDD6;Q66JR2;G3UYM0;G3UY59;G3UW37;G3UY87;G3V020	Stard10	ENSMUSG00000030688	STARD10
E9QLQ3;Q61409	Pde3b	ENSMUSG00000030671	PDE3B
P81117	Nucb2	ENSMUSG00000030659	NUCB2
B0LAE4;Q3UBA1;Q3TQE3;Q8C1Y9;Q80ZW9;Q3TIC7;Q3THR3;Q9JKW0	Arl6ip1	ENSMUSG00000030654	ARL6IP1
P54071	Idh2	ENSMUSG00000030541	IDH2
Q8C076;P59016	Vps33b	ENSMUSG00000030534	VPS33B
Q8CFZ2;Q62030;E9Q4D0;F6XJP7;H3BJL4	Pcsk6	ENSMUSG00000030513	PCSK6
Q7TMB8-2;Q7TMB8	Cyfip1	ENSMUSG00000030447	CFIP1
Q80XR5;P26369;Q505Q1;Q922I0;Q3KQM4	U2af2	ENSMUSG00000030435	U2AF2
Q3U3S0;P58404-2;P58404	Strn4	ENSMUSG00000030374	STRN4
Q8BJA6;Q3UY68;Q91YS8;Q3TDH8	Camk1	ENSMUSG00000030272	CAMK1
Q3UJN2;Q3U1C2;P60122	Ruvbl1	ENSMUSG00000030079	RUVBL1
Q5RKP4;Q91YQ5;Q8BMR3;Q3U900;Q99LY0	Rpn1	ENSMUSG00000030062	RPN1
Q9QZE5	Copg1	ENSMUSG00000030058	COPG1
Q3UME9;Q3U026;Q80UM7;Q3U950;Q3U8P9	Mogs	ENSMUSG00000030036	MOGS
E9QML5;Q61464-4;Q61464;E9QKZ7;Q61464-7;Q61464-2;Q61464-5;Q3TNM0;Q3TZK9;Q3TQM2;Q3TQ35	Zfp638	ENSMUSG00000030016	ZNF638
Q7TMN7	Anxa4	ENSMUSG00000029994	ANXA4
Q9CZD3	Gars	ENSMUSG00000029777	GARS1
Q3U9V4;P62880;E9QKR0;D3YZX3;D3Z1M1;D3Z1T4	Gnb2	ENSMUSG00000029713	GNB2
H3BKT0;H3BJN3;Q6AXG1;Q9JJB6;H3BJ26;H3BLJ7	Cux1	ENSMUSG00000029705	CUX1
P52946	Pdx1	ENSMUSG00000029644	PDX1
B2RTB0;Q3UHX2;Q1WWJ8	Pdap1	ENSMUSG00000029623	PDAP1
Q3TCE7;Q91Z25;Q9WV32;Q3U094;Q3TBA2	Arpc1b	ENSMUSG00000029622	ARPC1B
Q9R0Q6	Arpc1a	ENSMUSG00000029621	ARPC1A
P57759	Erp29	ENSMUSG00000029616	ERP29

Q3UY34	2210016L21Rik	ENSMUSG00000029559	C12orf43
Q9WTX8;Q9WTX8-2	Mad1l1	ENSMUSG00000029554	MAD1L1
Q8K370;Q9CRH8	Acad10	ENSMUSG00000029456	ACAD10
Q544B1;Q3UJW1;Q3U9J7;Q3TVM2;P47738;Q3U6I3	Aldh2	ENSMUSG00000029455	ALDH2
S4R2L4;B7ZNU2;S4R265;A2RTL5;S4R1M5	Rsrc2	ENSMUSG00000029422	RSRC2
D3YXR8;Q80U40-2;Q80U40	Rimbp2	ENSMUSG00000029420	RIMBP2
Q9JJ59;Q9JJ59-2	Abcb9	ENSMUSG00000029408	ABCB9
E9PYJ7;Q6ZPQ6-2;Q6ZPQ6;Q6NS55;Q3UEE4	Pitpnm2	ENSMUSG00000029406	PITPNM2
Q9D394-2	Rufy3	ENSMUSG00000029291	RUFY3
Q3TM92;Q91W96;Q3TI31	Anapc4	ENSMUSG00000029176	ANAPC4
Q9EQF6	Dpysl5	ENSMUSG00000029168	DPYSL5
Q2UZW7;Q6PER3	Mapre3	ENSMUSG00000029166	MAPRE3
Q99K41;Q3U254;Q3USG5;Q3UUU0	Emilin1	ENSMUSG00000029163	EMILIN1
E9Q1Q9;P97328;Q9CPP1;D3YVB6	Khk	ENSMUSG00000029162	KHK
Q9CRD0;Q9CRD0-2;Q9CRD0-3	Ociad1	ENSMUSG00000029152	OCIAD1
Q3TCW5;Q99J45;D3YUV1	Nrbp1	ENSMUSG00000029148	NRBP1
Q61074	Ppm1g	ENSMUSG00000029147	PPM1G
Q8BVL3	Snx17	ENSMUSG00000029146	SNX17
D3Z780;Q61749;Q61749-2	Eif2b4	ENSMUSG00000029145	EIF2B4
E9PX68;Q5BKS1;O54716;E9Q585;Q3UHY0;E9Q1Q0;Q3UUI2;Q6GQW1	Slc4a1ap	ENSMUSG00000029141	SLC4A1AP
B1AX98;E9PV22;Q505F5	Lrrc47	ENSMUSG00000029028	LRRC47
Q542V3;Q8VE97;Q8K3A8;A2A837	Srsf4	ENSMUSG00000028911	SRSF4
P48193;A2A841;P48193-2;A2A842;A2AD32;B6ZHC8	Epb41	ENSMUSG00000028906	EPB41
Q58E59;Q9D554	Sf3a3	ENSMUSG00000028902	SF3A3
Q3U5F4	Yrdc	ENSMUSG00000028889	YRDC
Q923G3;P47757-2;A2AMW0;P47757-4;Q3TVK4;Q3TRH8;P47757;F7CAZ6	Capzb	ENSMUSG00000028745	CAPZB
B1AU76;B1AU75;Q99MD9-2;Q99MD9	Nasp	ENSMUSG00000028693	NASP
Q540D7;Q9JII6;Q80XJ7;Q3UJW9;B1AXW3	Akr1a1	ENSMUSG00000028692	AKR1A1
P35700;B1AXW5;B1AXW6;Q3U9J9;B1AXW4	Prdx1	ENSMUSG00000028691	PRDX1
B1ARU4;E9PVY8;E9QA63;Q9QXZ0;E9QNP1;Q9QXZ0-3;Q9QXZ0-2;Q9QXZ0-4;F6Q750	Macf1	ENSMUSG00000028649	MACF1
P32020;P32020-2	Scp2	ENSMUSG00000028603	SCP2
Q3TLP5;Q3TLP5-2;F6YTG0;Q3TLP5-3	Echdc2	ENSMUSG00000028601	ECHDC2
E9PX48;A2A9M5;Q8R1A4-2;Q8R1A4	Dock7	ENSMUSG00000028556	DOCK7
A2ACP1-2;A2ACP1	Ttc39a	ENSMUSG00000028555	TTC39A
Q3U054;Q9D153;Q60772	Cdkn2c	ENSMUSG00000028551	CDKN2C
Q7TT37	Elp1	ENSMUSG00000028431	ELP1
Q9D7S9	Chmp5	ENSMUSG00000028419	CHMP5
F6TCF9;Q60739-2;Q60739;Q9CUY1	Bag1	ENSMUSG00000028416	BAG1
Q5NTY0;Q3TK61;P63037;B1AXY1;B1AXY0	Dnaja1	ENSMUSG00000028410	DNAJA1
Q9DCV4;A2AGJ2	Rmdn1	ENSMUSG00000028229	RMDN1
Q9CQB5	Cisd2	ENSMUSG00000028165	CISD2
Q8K2I4	Manba	ENSMUSG00000028164	MANBA
P25799;P25799-4;P25799-2;P25799-3	Nfkb1	ENSMUSG00000028163	NFKB1
P48678;P48678-2;P48678-3	Lmna	ENSMUSG00000028063	LMNA
Q9JHS3;D3YTS4	Lamtor2	ENSMUSG00000028062	LAMTOR2
H3BJU7;H3BJX8;H3BJ45;H3BJ40;H3BKH9;Q60875-5;Q60875-4;Q60875;Q3TYZ4;Q60875-2;Q60875-3	Arhgef2	ENSMUSG00000028059	ARHGEF2
B9EJR4;O35387	Hax1	ENSMUSG00000027944	HAX1
Q8CAQ1;G3X9Q0;Q9JKP5;Q8CHF5	Mbnl1	ENSMUSG00000027763	MBNL1
Q3TEB9;Q6NX62;Q6PCW8;Q546F8;Q571G2;Q9D753;F6SGT4;D3YYN3	Exosc8	ENSMUSG00000027752	EXOSC8
P14246	Slc2a2	ENSMUSG00000027690	SLC2A2
Q541E2;Q3TWM2;P51855;Q8R436	Gss	ENSMUSG00000027610	GSS
Q8N9U3;Q8C1A8;Q8C141;A2AQN4;Q9QXG4;Q8C113;A2AQN5	Acss2	ENSMUSG00000027605	ACSS2
Q6P289;Q571M5;Q8C863;Q8C863-2	Itch	ENSMUSG00000027598	ITCH
Q8VDM1;F7C2Y9	Zgpat	ENSMUSG00000027582	ZGPAT
B5B2P6;B5B2Q2;B5B2P7;Q60591-4;Q60591-2;Q60591;B5B2P8;B5B2Q4;Q3TTU8;B5B2Q6;A2AQC8;B5B2R5;Q8C443;Q6P3F6	Nfatc2	ENSMUSG00000027544	NFATC2
P63094;Q6R0H7;P63094-3	Gnas	ENSMUSG00000027523	GNAS
Q3TYS4;Q9D662;Q3TAW4;Q3UKB4;Q3TIS3;Q8CDS4	Sec23b	ENSMUSG00000027429	SEC23B
Q80VD1	Fam98b	ENSMUSG00000027349	FAM98B
Q3UA17;Q791V5;A2AFW6;Q9D050;Q05C68	Mtch2	ENSMUSG00000027282	MTCH2
Q99K28;Q99K28-2	Arfgap2	ENSMUSG00000027255	ARFGAP2
A2ARP8;Q9QYR6;Q9QYR6-2	Map1a	ENSMUSG00000027254	MAP1A
P27773	Pdia3	ENSMUSG00000027248	PDIA3
Q8BQW4;A2AH25;Q5FWK3;Q8C5A0	Arhgap1	ENSMUSG00000027247	ARHGAP1
Q3V3N6;P61202;P61202-2;A2AQE4;Q3UK65	Cops2	ENSMUSG00000027206	COPS2
A2AQ53;O88840;Q61554;Q60784	Fbn1	ENSMUSG00000027204	FBN1
Q8C6E3;Q542K4;Q3UZE7;Q3TVZ1;P24270;Q3UF58;Q91XI2	Cat	ENSMUSG00000027187	CAT
A2AIX1;E9QAT4;Q811L5;Q80U43;F7BPW6	Sec16a	ENSMUSG00000026924	SEC16A
Q3TUI3;Q8K2F0;Q05DR7;Q4G5Y4;Q5CCJ9;Q8K2F0-2;A2AKA9;Q53TY6	Brd3	ENSMUSG00000026918	BRD3
Q91WM1-2;Q91WM1;Q8C5B7	Strbp	ENSMUSG00000026915	STRBP
Q6PAC1;P13020-2;Q3UCW8;P13020;Q3U9Q8;Q3TGJ9	Gsn	ENSMUSG00000026879	GSN
Q6Q477;D1FNM9;Q32ME1;F7AAP4;D1FNM8;H2BL43;E9Q828	Atp2b4	ENSMUSG00000026463	ATP2B4
A0A087WRY3;Q80XU3	Nucks1	ENSMUSG00000026434	NUCKS1
Q3TDQ5;G9M4M6;Q8C0J2-2;Q8C0J2-5;Q8C0J2;Q8C0J2-3;Q8C0J2-4;Q3TQX8	Atg16l1	ENSMUSG00000026289	ATG16L1
Q3V2C6;Q3V1K9;P31001	Des	ENSMUSG00000026208	DES
Q9JKY0	Cnot9	ENSMUSG00000026174	CNOT9
E9PUC4;Q6NSW3-2;Q6NSW3;Q6NSW3-3;Q6NSW3-4	Sphkap	ENSMUSG00000026163	SPHKAP
Q9JKX6	Nudt5	ENSMUSG00000025817	NUDT5
P09055;P09055-2	Itgb1	ENSMUSG00000025809	ITGB1
Q3TIC8;Q9CZ13;Q3THM1;Q8K2S8	Uqcrc1	ENSMUSG00000025651	UQCRC1
Q8R4N0	Clybl	ENSMUSG00000025545	CLYBL
Q3UUH0;Q91YI0;E0CXM2;E0CY49	Asl	ENSMUSG00000025533	ASL
O35566	Cd151	ENSMUSG00000025510	CD151
P99027	Rplp2	ENSMUSG00000025508	RPLP2
B2RT97;Q9WVJ2;E9Q5I9	Psmd13	ENSMUSG00000025487	PSMD13
Q3TIR3	Ric8a	ENSMUSG00000025485	RIC8A
O35153;I6L979	Bet1l	ENSMUSG00000025484	BET1L
Q8R2K1;D3YWS7;F6SJM7;Q8R2K1-2;Q8R2K1-3;Q8R2K1-5;Q8R2K1-4;F6X9P4	Fuom	ENSMUSG00000025466	FUOM
Q03265;D3Z6F5	Atp5a1	ENSMUSG00000025428	ATP5F1A
Q3TPZ5;Q99KJ8	Dctn2	ENSMUSG00000025410	DCTN2
Q99K87;Q3TFD0;Q9CZN7	Shmt2	ENSMUSG00000025403	SHMT2
Q3UID0;Q6PDG5-2;Q6PDG5	Smarcc2	ENSMUSG00000025369	SMARCC2
Q3TGU7;P50580;Q05BN2;Q3UMW2;D3YVH7	Pa2g4	ENSMUSG00000025364	PA2G4
Q497N1;P62855	Rps26	ENSMUSG00000025362	RPS26
P70122;F6TN03	Sbds	ENSMUSG00000025337	SBDS
Q9QXE7	Tbl1x	ENSMUSG00000025246	TBL1X
Q9JHQ5;Q8CDG8;Q3UHL8;F6VG18;F6VTH5	Lztfl1	ENSMUSG00000025245	LZTFL1
Q8VDC1	Fyco1	ENSMUSG00000025241	FYCO1
Q9EQQ9-3;Q9EQQ9	Oga	ENSMUSG00000025220	OGA
Q8CI33;Q8CI33-2	Cwf19l1	ENSMUSG00000025200	CWF19L1
Q91X78	Erlin1	ENSMUSG00000025198	ERLIN1
Q6P264;Q7TQJ3;Q9ER35	Fn3k	ENSMUSG00000025175	FN3K

Q3TWE3;Q3THC3;Q3TF72;P09103;Q3URP6;Q3UBY9;Q3UJA8;Q3UA23;Q3TIM0;Q3TGS0;Q3UDR2;Q3U738;Q3TT76	P4hb	ENSMUSG00000025130	P4HB
G3X9J6;E9Q9M1;Q3V1L4	Nt5c2	ENSMUSG00000025041	NT5C2
O89116	Vti1a	ENSMUSG00000024983	VTI1A
Q61823	Pdcd4	ENSMUSG00000024975	PDCD4
Q3UWS9;Q3U7H9;P99029-2;P99029;G3UZJ4;H3BJQ7;Q9D6X2	Prdx5	ENSMUSG00000024953	PRDX5
R4H4V1;R4H4Y7;Q9EQC5	Scyl1	ENSMUSG00000024941	SCYL1
Q91XB7	Yif1a	ENSMUSG00000024875	YIF1A
Q0PD66;Q9D1G1	Rab1b	ENSMUSG00000024870	RAB1B
Q3UJB0;Q3UAI4;Q80W39;Q3UBH2;Q3UQU5;Q8BL33	Sf3b2	ENSMUSG00000024853	SF3B2
Q91Z50;Q8R069;Q8C952;Q3TGH6;Q8C5X6;Q99M86;P39749	Fen1	ENSMUSG00000024742	FEN1
P30677;Q8CBT5;Q8C3M7	Gna14	ENSMUSG00000024697	GNA14
Q3UHH5;P21279	Gnaq	ENSMUSG00000024639	GNAQ
Q06180-2;Q06180;D3Z6W2	Ptpn2	ENSMUSG00000024539	PTPN2
Q9D8V7;Q8BM48	Sec11c	ENSMUSG00000024516	SEC11C
Q3TKB7;Q3THT9;Q99N84;G3UYQ9;G3UYX8;Q542W5;G3UX79;Q99N84-2	Mrps18b	ENSMUSG00000024436	MRPS18B
P36916;A2VDH5;Q52KE3;P36916-2	Gnl1	ENSMUSG00000024429	GNL1
Q5DTJ4;Q7TSC1	Prrc2a	ENSMUSG00000024393	PRRC2A
N0E4C0;P67871;N0E4C5;G3UXG7;G3UZJ5;N0E463;G3UXU2	Csnk2b	ENSMUSG00000024387	CSNK2B
Q3UIA1;P19426-2;P19426;G3UY39	Nelfe	ENSMUSG00000024369	NELFE
Q61228;A0A068BGU5;Q61230;Q61229;Q61227	Tap2	ENSMUSG00000024339	TAP2
A0A068BIT8;P28063;G3UZW8	Psmb8	ENSMUSG00000024338	PSMB8
B2RS09;Q7JJ13-2;Q7JJ13;U3KLT0	Brd2	ENSMUSG00000024335	BRD2
Q14C53;A0A068BIT0;Q31125	Slc39a7	ENSMUSG00000024327	SLC39A7
A0A068BGT0;Q8C754;G3UY33;Q3V3A4;Q8C754-2	Vps52	ENSMUSG00000024319	VPS52
Q5XW48;Q3U9A3;Q3TED6;Q9D679;Q91WI5;Q3TCU5;A0A068BIS1;Q9R233-2;Q9R233;Q5XW51;Q5XW49;Q5XW52;G3UZZ2;Q5XW46	Tapbp	ENSMUSG00000024308	TAPBP
Q4FJN2;Q64378;Q3TX72	Fkbp5	ENSMUSG00000024222	FKBP5
I1E4X7;Q9JI46;H3BLR8;B2KF67	Nudt3	ENSMUSG00000024213	NUDT3
D3Z4C9;Q9CQY6;D3Z4D6	Uqcc2	ENSMUSG00000024208	UQCC2
D5MCW4;Q9CQ89	Cuta	ENSMUSG00000024194	CUTA
Q3TV90;Q9CYI4;Q05D11;D3Z765;Q9CYI4-2	Luc7l	ENSMUSG00000024188	LUC7L
D3Z6P0-2;D3Z6P0	Pdia2	ENSMUSG00000024184	PDIA2
Q059U9;Q9DBR0	Akap8	ENSMUSG00000024045	AKAP8
Q9DBC3	Cmtr1	ENSMUSG00000024019	CMTR1
Q9CPP6;Q9CX78	Ndufa5	ENSMUSG00000023089	NDUFA5
Q3UH60;D3Z5G8;Q3UH60-2	Dip2b	ENSMUSG00000023026	DIP2B
Q3UT02;E9Q066;G3X9Q6;Q8BWW4	Larp4	ENSMUSG00000023025	LARP4
Q9ERG0;Q8C7S2;Q8CD09;Q9ERG0-2;Q8C3R7;Q8BT15	Lima1	ENSMUSG00000023022	LIMA1
Q64737;Q3UJP8;Q3TH49;Q64737-2	Gart	ENSMUSG00000022962	GART
H9KV00;Q9QX47-3;Q9QX47;H9KV15;H9KV01;Q9QX47-4;Q9QX47-2	Son	ENSMUSG00000022961	SON
Q64685;Q9JJM6	St6gal1	ENSMUSG00000022885	ST6GAL1
Q52KC1;P10630;Q8BTU6;E9Q561	Eif4a2	ENSMUSG00000022884	EIF4A2
Q80X54;Q91YJ2	Snx4	ENSMUSG00000022808	SNX4
Q8K0F1	Tbc1d23	ENSMUSG00000022749	TBC1D23
Q99K01-2	Pdxdc1	ENSMUSG00000022680	PDXDC1
Q8C3X8	Lmf2	ENSMUSG00000022614	LMF2
Q9DCC4	Pycrl	ENSMUSG00000022571	PYCR3
Q80T84;D3Z624;G3XA21;E0CZ22	Mroh1	ENSMUSG00000022558	MROH1
Q8VDD5;Q3UFT0	Myh9	ENSMUSG00000022443	MYH9
Q8BGH2	Samm50	ENSMUSG00000022437	SAMM50
Q921M7	Cyrib	ENSMUSG00000022378	CYRIB
Q8BPS4	Gpr180	ENSMUSG00000022131	GPR180
Q9EPK7-2;Q9EPK7;E9PUW7	Xpo7	ENSMUSG00000022100	XPO7
P98063;Q6P550;Q570Z4	Bmp1	ENSMUSG00000022098	BMP1
Q3TT94;Q6P1F6;Q571J7;Q3TPC5;Q9CWU3	Ppp2r2a	ENSMUSG00000022052	PPP2R2A
E9Q774;E9Q777;Q6ZQ80;Q8BSJ2	Akap11	ENSMUSG00000022016	AKAP11
P40142	Tkt	ENSMUSG00000021957	TKT
Q3TVS6;P10605;Q3TC17;Q6LAF6	Ctsb	ENSMUSG00000021939	CTSB
Q9D958	Spcs1	ENSMUSG00000021917	SPCS1
Q8VE38-2;Q8VE38	Oxnad1	ENSMUSG00000021906	OXNAD1
Q14BR4;P61750;Q9DD04;E9Q798	Arf4	ENSMUSG00000021877	ARF4
D3Z7V3;H7BX64;Q3URD3-2;Q3URD3;F8WIH0;F6UV57;F6YCM8;Q3URD3-5	Slmap	ENSMUSG00000021870	SLMAP
Q64727	Vcl	ENSMUSG00000021823	VCL
Q923F9;E9QPX3;Q9CXZ1;Q9CTT4	Ndufs4	ENSMUSG00000021764	NDUFS4
Q99JI4;Q8C1T2	Psmd6	ENSMUSG00000021737	PSMD6
Q9D0G0	Mrps30	ENSMUSG00000021731	MRPS30
Q544T5;P00375	Dhfr	ENSMUSG00000021707	DHFR2
B9EKK3	Iqgap2	ENSMUSG00000021676	IQGAP2
Q8BSX8;Q9EQG9-2;Q9EQG9;Q9EQG9-3	Cert1	ENSMUSG00000021669	CERT1
Q32MU0;P63239	Pcsk1	ENSMUSG00000021587	PCSK1
Q9CZL5	Pcbd2	ENSMUSG00000021496	PCBD2
Q9DBH5	Lman2	ENSMUSG00000021484	LMAN2
E9QKB2;Q9JKS5	Habp4	ENSMUSG00000021476	HABP4
Q3TV94;Q52PE3;Q9CY50	Ssr1	ENSMUSG00000021427	SSR1
D3Z030;Q6EDY6-3;Q6EDY6;F7AI27	Carmil1	ENSMUSG00000021338	CARMIL1
Q91WD9	Scgn	ENSMUSG00000021337	SCGN
Q60803;Q3UHM2;Q3UHJ1	Traf3	ENSMUSG00000021277	TRAF3
Q3U6U7;P32921-2;Q3UDG2;Q4FJZ4;P32921	Wars	ENSMUSG00000021266	WARS1
Q3UZJ4;Q61151	Ppp2r5e	ENSMUSG00000021051	PPP2R5E
Q91YP0	L2hgdh	ENSMUSG00000020988	L2HGDH
Q8CCP0;Q8CCP0-2;Q8CCP0-3	Nemf	ENSMUSG00000020982	NEMF
Q543F1;Q3U5Q3;A2AH85;Q6A0E3;O08810;G3UZ34;Q3TMY8;Q7TMX4	Eftud2	ENSMUSG00000020929	EFTUD2
P42232	Stat5b	ENSMUSG00000020919	STAT5B
Q5SUR0	Pfas	ENSMUSG00000020899	PFAS
Q8CHR4;O35619;B0QZN5;P63044	Vamp2	ENSMUSG00000020894	VAMP2
Q5F239;P62254;D6RES1	Ube2g1	ENSMUSG00000020794	UBE2G1
B7ZP20	Ankfy1	ENSMUSG00000020790	ANKFY1
Q04690-2;Q04690;Q04690-4;Q04690-3	Nf1	ENSMUSG00000020716	NF1
Q4FJL0;P61027;Q3U621	Rab10	ENSMUSG00000020671	RAB10
Q542A1;Q61334	Bcap29	ENSMUSG00000020650	BCAP29
A9E3L2;Q9Z2I2;Q80YE1;Q810R7	Fkbp1b	ENSMUSG00000020635	FKBP1B
Q9DBC7;Q3TYK4;Q8C3Z4;Q3UBA7;A2AI69;F8S0Y0	Prkar1a	ENSMUSG00000020612	PRKAR1A
Q9QXB9	Drg2	ENSMUSG00000020537	DRG2
P28661-5;P28661-4;P28661-3;P28661-2;P28661	septin4	ENSMUSG00000020486	SEPTIN4
Q62418-3;Q62418-2;Q62418	Dbnl	ENSMUSG00000020476	DBNL
O35654;A8Y5G7	Pold2	ENSMUSG00000020471	POLD2
Q3U2G2;Q571M2;Q61316	Hspa4	ENSMUSG00000020361	HSPA4
Q8R1K4;Q8R1K4-2;F8WHK6;Q8R1K4-3	Phykpl	ENSMUSG00000020359	PHYKPL
Q62261	Sptbn1	ENSMUSG00000020315	SPTBN1
Q9JMH6-2;Q9JMH6	Txnrd1	ENSMUSG00000020250	TXNRD1
Q3UB66;Q0PD67;P62821	Rab1a	ENSMUSG00000020149	RAB1A
Q80YD1	Supv3l1	ENSMUSG00000020079	SUPV3L1

Q5BKP5;Q99MJ9;Q8BRU5	Ddx50	ENSMUSG00000020076	DDX50
Q9JIK5;Q6PCP0;Q3ULC7;Q9CWZ5;Q8K2L4	Ddx21	ENSMUSG00000020075	DDX21
Q8CH18;Q8CH18-3	Ccar1	ENSMUSG00000020074	CCAR1
Q3TGM7;Q69ZS7;Q3UJ02;Q69ZS7-2	Hbs1l	ENSMUSG00000019977	HBS1L
Q3TNH0;Q61029-3;Q61029-2;Q61033-2	Tmpo	ENSMUSG00000019961	TMPO
K3W4Q9;Q8BH60-2;Q8BH60	Gopc	ENSMUSG00000019861	GOPC
Q8R344	Ccdc12	ENSMUSG00000019659	CCDC12
Q9Z1N5;Q3TB18	Ddx39b	ENSMUSG00000019432	DDX39B
Q6NXX6;K3W4T3;Q9Z1G4-3;Q9Z1G4-2;Q3TXT5;Q9Z1G4;Q3TY98	Atp6v0a1	ENSMUSG00000019302	ATP6V0A1
P08249	Mdh2	ENSMUSG00000019179	MDH2
Q3UCY7;Q3TWN7;Q571E2;Q9R1Q9;Q3TT23;Q3THZ3;Q3UWN7;Q3TKX1	Atp6ap1	ENSMUSG00000019087	ATP6AP1
Q8BXJ6;Q8BGV0;D3YV21	Nars2	ENSMUSG00000018995	NARS2
Q9JLI8	Sart3	ENSMUSG00000018974	SART3
P68510	Ywhah	ENSMUSG00000018965	YWHAH
Q9D0I9;Q3TVC5;Q3UAZ3	Rars	ENSMUSG00000018848	RARS1
D3Z041;P41216	Acsl1	ENSMUSG00000018796	ACSL1
Q6P5B5;Q9WVR4	Fxr2	ENSMUSG00000018765	FXR2
E9PVP3;Q5F2B1;Q8C9V6;Q8R0J2;F6XX36;Q9R0Q9	Mpdu1	ENSMUSG00000018761	MPDU1
Q9JHH9;Q9CTG7;F2Z4A2	Copz2	ENSMUSG00000018672	COPZ2
Q3U506;Q3TLJ5;Q99LM2;Q3TSS9	Cdk5rap3	ENSMUSG00000018669	CDK5RAP3
P83917;Q7TPM0;Q9CYJ8	Cbx1	ENSMUSG00000018666	CBX1
Q3TWY6;Q9Z160;Q3TR89;Q3TAY0;Q3U7X8;Q810S7;Q3TYM3	Cog1	ENSMUSG00000018661	COG1
Q91XF0	Pnpo	ENSMUSG00000018659	PNPO
P50544;B1AR28;Q3UJR6	Acadvl	ENSMUSG00000018574	ACADVL
A2A5Y6;P10637;P10637-6	Mapt	ENSMUSG00000018411	MAPT
A2A5N2;Q9CQV8;A2A5N1	Ywhab	ENSMUSG00000018326	YWHAB
Q3USC7;Q8VE33;A2A5H8	Gdap1l1	ENSMUSG00000017943	GDAP1L1
Q3UQB4;A2BFB1;Q8K0H8;A2BFB0;O08609-3;O08609;A2BFB2;O08609-2	Mlx	ENSMUSG00000017801	MLX
E9PUE7;Q5SSL4;Q5SSL4-2;Q5SSL4-4;Q5SSL4-3	Abr	ENSMUSG00000017631	ABR
H3BIW0;G3X8T2;Q0P678	Zc3h18	ENSMUSG00000017478	ZC3H18
B2RX66;Q5F2E8;Q3UUG1	Taok1	ENSMUSG00000017291	TAOK1
Q2M4I9;A2A4A6;Q62077;Q3UZ68	Plcg1	ENSMUSG00000016933	PLCG1
Q3UJ84;Q3U417;Q8C8U0;Q8C8U0-3;Q8C8U0-2	Ppfibp1	ENSMUSG00000016487	PPFIBP1
Q9D8S9	Bola1	ENSMUSG00000015943	BOLA1
Q9QZQ8	Macroh2a1	ENSMUSG00000015937	MACROH2A1
V9GXE6;I6L9E0;Q3U3J6;A2ALA6;P09925	Surf1	ENSMUSG00000015790	SURF1
Q3THX4;P97390	Vps45	ENSMUSG00000015747	VPS45
Q8BIW1	Prune1	ENSMUSG00000015711	PRUNE1
Q4FJQ8;Q3UAX2;Q8C562;Q3UC81;Q3UB98;Q3UB54;Q3U841;Q3U784;Q3U5U0;P11152;Q3UCZ2;Q3UCD4;Q3UC44;Q3UBE9;Q3U715;Q3UCH4;Q3U6S8	Lpl	ENSMUSG00000015568	LPL
P50396	Gdi1	ENSMUSG00000015291	GDI1
Q9CR70;J3JS94	Lage3	ENSMUSG00000015289	LAGE3
A1BN54;Q7TPR4	Actn1	ENSMUSG00000015143	ACTN1
Q571E4;Q8CC47	Galns	ENSMUSG00000015027	GALNS
Q3URE1	Acsf3	ENSMUSG00000015016	ACSF3
Q545Q2;Q64310;Q3U7E6;E0CXD9;F7CH13	Surf4	ENSMUSG00000014867	SURF4
Q505D1	Ankrd28	ENSMUSG00000014496	ANKRD28
B7ZNX2;P53995;A2ATQ5;Q3UE43;Q3TP10	Anapc1	ENSMUSG00000014355	ANAPC1
Q3UE37	Ube2z	ENSMUSG00000014349	UBE2Z
Q9D5T0;Q9D9C1	Atad1	ENSMUSG00000013662	ATAD1
B2RQC6;E9QAI5;G3UWN2;B2RQC6-2;Q6P9L1	Cad	ENSMUSG00000013629	CAD
Q91WD5;D3YXT0;F6RJ83	Ndufs2	ENSMUSG00000013593	NDUFS2
Q8C4Y3;Q69ZP4	Nelfb	ENSMUSG00000013465	NELFB
Q3U7Z6;Q9DBJ1;Q6NWV5	Pgam1	ENSMUSG00000011752	PGAM1
Q8CH02	Sugp1	ENSMUSG00000011306	SUGP1
D3Z5M2;Q99LF8	Pabpc4	ENSMUSG00000011257	PABPC4
Q80WQ2;Q8CCX6;Q8C907	Vac14	ENSMUSG00000010936	VAC14
Q8BKZ9	Pdhx	ENSMUSG00000010914	PDHX
Q9ER72;Q3UXN3	Cars	ENSMUSG00000010755	CARS1
P54731	Faf1	ENSMUSG00000010517	FAF1
Q9CW46	Raver1	ENSMUSG00000010205	RAVER1
Q61686	Cbx5	ENSMUSG00000009575	CBX5
Q8BFY9-2;Q8BFY9;Q3TKD0	Tnpo1	ENSMUSG00000009470	TNPO1
Q64332	Syn2	ENSMUSG00000009394	SYN2
Q5SVG5;Q5SVG4;O35643;Q8CC13;Q3TVN4;Q3U1K9	Ap1b1	ENSMUSG00000009090	AP1B1
Q561N5;F6YVP7;P62270;S4R1N6;Q3TW65	Rps18	ENSMUSG00000008668	RPS18
Q3TMH2	Scrn3	ENSMUSG00000008226	SCRN3
Q564F4;Q3TII0;P80315;Q3UJZ8;G5E839	Cct4	ENSMUSG00000007739	CCT4
B2RRS4;E9PWV7;Q923K4;D6RDC6;Q923K4-2	Gtpbp3	ENSMUSG00000007610	GTPBP3
Q3UKQ5;Q3UF03;P24668	M6pr	ENSMUSG00000007458	M6PR
Q3U9X2;Q9ES84;O35901;O35900;Q9EP83	Lsm2	ENSMUSG00000007050	LSM2
Q542F1;Q9Z1Q5;Q3TIP8	Clic1	ENSMUSG00000007041	CLIC1
Q99LD8;O08972	Ddah2	ENSMUSG00000007039	DDAH2
Q3UL64;O35657	Neu1	ENSMUSG00000007038	NEU1
Q790I0;Q9Z1Q9;Q7TPT7;Q3U3D3;G3UY93;Q3TII4	Vars	ENSMUSG00000007029	VARS1
E9Q9M5;J3KMM1;Q3UJD6-2;Q3UJD6	Usp19	ENSMUSG00000006676	USP19
P08030	Aprt	ENSMUSG00000006589	APRT
Q9CVB6;Q3UA52;Q4FZG5;D3YXG6	Arpc2	ENSMUSG00000006304	ARPC2
P62814	Atp6v1b2	ENSMUSG00000006273	ATP6V1B2
Q922Z3;Q3UPJ8;Q3TK29;Q9CQN1;Q922R9;Q3TSG8	Trap1	ENSMUSG00000005981	TRAP1
P99026	Psmb4	ENSMUSG00000005779	PSMB4
Q3U8E7;P18155	Mthfd2	ENSMUSG00000005667	MTHFD2
M4TKR7;P15208	Insr	ENSMUSG00000005534	INSR
P37040;Q05DV1	Por	ENSMUSG00000005514	POR
Q9DCT2	Ndufs3	ENSMUSG00000005510	NDUFS3
P28659-4;P28659-2;P28659-3;P28659	Celf1	ENSMUSG00000005506	CELF1
Q9R099;Q9CY49	Tbl2	ENSMUSG00000005374	TBL2
Q99MZ3;Q99MZ3-4;Q99MZ3-3;H9U1Q1;Q99MZ3-5;Q99MZ3-2	Mlxipl	ENSMUSG00000005373	MLXIPL
Q8C2D2;P70362;Q9CWQ7;Q9CZJ3	Ufd1	ENSMUSG00000005262	UFD1
Q9Z186	G6pc2	ENSMUSG00000005232	G6PC2
O08847;P08775	Polr2a	ENSMUSG00000005198	POLR2A
Q61171;Q5M9N9;D3Z4A4	Prdx2	ENSMUSG00000005161	PRDX2
O88569;O88569-2;O88569-3;B7ZP22	Hnrnpa2b1	ENSMUSG00000004980	HNRNPA2B1
Q9R0N5	Syt5	ENSMUSG00000004961	SYT5
Q3U9G9	Lbr	ENSMUSG00000004880	LBR
Q8R1V4;Q5SVW9	Tmed4	ENSMUSG00000004394	TMED4
Q6ZQ84;Q9JLV5;E9Q4T8	Cul3	ENSMUSG00000004364	CUL3
Q91V01	Lpcat3	ENSMUSG00000004270	LPCAT3
Q542P8;O35130	Emg1	ENSMUSG00000004268	EMG1
Q545V3;Q3UJ20;P17183;D3Z6E4;Q922A0	Eno2	ENSMUSG00000004267	ENO2
Q3V235;O35129;F6QPR1	Phb2	ENSMUSG00000004264	PHB2
Q544R7;Q3U6W4;O70252;D3YX62	Hmox2	ENSMUSG00000004070	HMOX2

Q3TY95;Q60823;F8WHG5;Q8CE74;D3YXM7;D3Z3N2	Akt2	ENSMUSG00000004056	AKT2
Q3ULI4;Q3U5Q4;P42227;Q6GU23;P42227-2;B7ZC18;Q3U6S9	Stat3	ENSMUSG00000004040	STAT3
P62918;Q3UJS0;Q3THC7;Q9Z237	Rpl8	ENSMUSG00000003970	RPL8
Q542Y0;Q64669;Q99KL8	Nqo1	ENSMUSG00000003849	NQO1
B2MWM9;P14211;Q3UWP8	Calr	ENSMUSG00000003814	CALR
Q60759;Q8BVD4	Gcdh	ENSMUSG00000003809	GCDH
Q8C0C7;E9PWY9;Q8BJG2;Q8BXN0;Q4FJQ2	Farsa	ENSMUSG00000003808	FARSA
Q9Z2X8;Q05DM3;Q3UWI4	Keap1	ENSMUSG00000003308	KEAP1
Q8CHW4	Eif2b5	ENSMUSG00000003235	EIF2B5
Q3TRJ7;Q62419;Q3U3C4	Sh3gl1	ENSMUSG00000003200	SH3GL1
P46414;Q4FJM2	Cdkn1b	ENSMUSG00000003031	CDKN1B
Q6GTX3;Q4FK40;Q3UBS0;Q3TXU4;P08226;Q3TX45;Q3UEE7;G3UWN5	Apoe	ENSMUSG00000002985	APOE
Q8VBZ3	Clptm1	ENSMUSG00000002981	CLPTM1
Q99K86;Q9R069;Q8BGB4	Bcam	ENSMUSG00000002980	BCAM
Q3UMU9;Q3UMU9-3;Q3UMU9-4;Q3UMU9-2	Hdgfl2	ENSMUSG00000002833	HDGFL2
Q9CQW1	Ykt6	ENSMUSG00000002741	YKT6
Q9D0K8;Q5RL57;Q3TLG2;Q9R0L7	Akap8l	ENSMUSG00000002625	AKAP8L
P28028	Braf	ENSMUSG00000002413	BRAF
Q9CQ56;Q5I940;Q05CJ0;Q9CQ56-2	Use1	ENSMUSG00000002395	USE1
Q8K4Z5;Q3TVM1	Sf3a1	ENSMUSG00000002129	SF3A1
P24638;Q3UZN1;Q3U4F3	Acp2	ENSMUSG00000002103	ACP2
Q3U8Y7;Q3TKG4;O88685;Q3TKC2;A2AGN7;B7ZCF1;A0A087WPH7;Q3UD94	Psmc3	ENSMUSG00000002102	PSMC3
Q3U9U5;Q61335	Bcap31	ENSMUSG00000002015	BCAP31
Q3TKM5;Q3TGZ3;P70404;Q684I8	Idh3g	ENSMUSG00000002010	IDH3G
O08579;Q3THM8;I7HJS1;B7FAU5	Emd	ENSMUSG00000001964	EMD
Q99LL5;E9QAL6;Q9CTC0;Q9CSK2;Q8BW04	Pwp1	ENSMUSG00000001785	PWP1
Q9DBL7	Coasy	ENSMUSG00000001755	COASY
O88325;O54752	Naglu	ENSMUSG00000001751	NAGLU
P99024	Tubb5	ENSMUSG00000001525	TUBB
Q11011;E9Q039;F6QYF8;E9Q6F4	Npepps	ENSMUSG00000001441	NPEPPS
Q3TFE8;Q7TSZ6;P70168;Q3UHW8	Kpnb1	ENSMUSG00000001440	KPNB1
Q3TW51;Q78PY7;Q3UZI3;Q3TRW3	Snd1	ENSMUSG00000001424	SND1
E9QKT0;Q63943-2;Q921S6;Q63943;Q3URR2;E9Q5E0	Mef2d	ENSMUSG00000001419	MEF2D
Q3U4U6;P80318;E9Q133;Q3U0I3;F6Q609	Cct3	ENSMUSG00000001416	CCT3
D3Z4P2;P59481	Lman2l	ENSMUSG00000001143	LMAN2L
Q9D689;Q6P1F5;Q6ZQ77;Q9JKY5;Q80UP1	Hip1r	ENSMUSG00000000915	HIP1R
P47963;Q5RKP3	Rpl13	ENSMUSG00000000740	RPL13
D3YZN4;Q7TNG0;D3Z1Z1;B2RQY8;Q3ULF4;D3YXB7;F6W695	Spg7	ENSMUSG00000000738	SPG7
B2RPS1;Q0PD56;P61021;Q8C458	Rab5b	ENSMUSG00000000711	RAB5B
Q545N7;P30275;A2ARP5	Ckmt1	ENSMUSG00000000308	CKMT1B
D3Z596;D3YWU5;D3Z595	Ins2	ENSMUSG00000000215	INS
P24529;Q3UTB3;E9Q9G5	Th	ENSMUSG00000000214	TH